CHAPTER# 3

OPTICAL FIBER COMMUNICATION

1.2 The general system

An optical fiber communication system is similar in basic concept to any type of communication system. A block schematic of a general communication system is shown in Figure 1.2(a), the function of which is to convey the signal from the information source over the transmission medium to the destination. The communication system therefore consists of a transmitter or modulator linked to the information source, the transmission medium, and a receiver or demodulator at the destination point. In electrical communications the information source provides an electrical signal, usually derived from a message signal which is not electrical (e.g. sound), to a transmitter comprising electrical and electronic components which converts the signal into a suitable form for propagation over the transmission medium. This is often achieved by modulating a carrier, which, as mentioned previously, may be an electromagnetic wave. The transmission medium can consist of a pair of wires, a coaxial cable or a radio link through free space down which the signal is transmitted to the receiver, where it is transformed into the original electrical information signal (demodulated) before being passed to the destination. However, it must be noted that in any transmission medium the signal is attenuated, or suffers loss, and is subject to degradations due to contamination by random signals and noise, as well as possible distortions imposed by mechanisms within the medium itself. Therefore, in any communication system there is a maximum permitted distance between the transmitter and the receiver beyond which the system effectively ceases to give intelligible communication. For long-haul applications these factors necessitate the installation of repeaters or line amplifiers

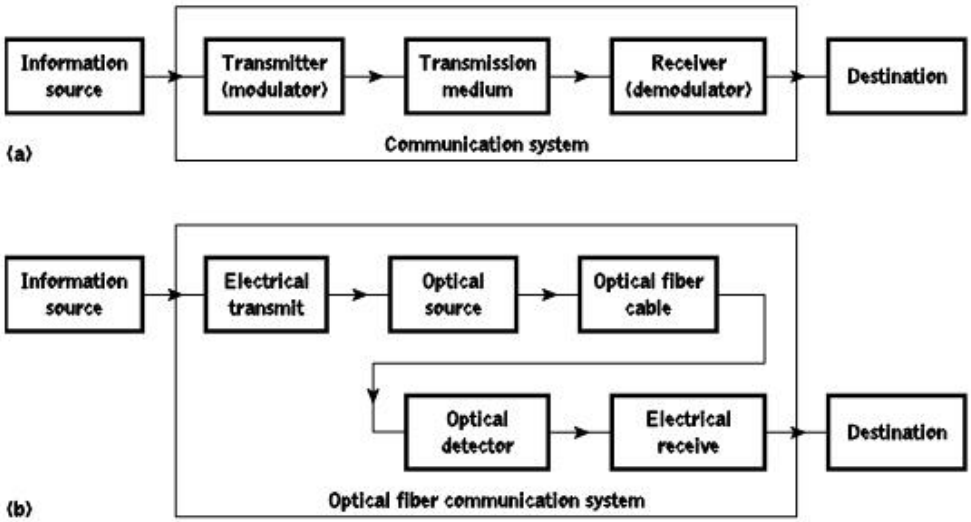

Figure 1.2 (a) The general communication system. (b) The optical fiber communication system

(see Sections 12.4 and 12.10) at intervals, both to remove signal distortion and to increase signal level before transmission is continued down the link.

For optical fiber communications the system shown in Figure 1.2(a) may be considered in slightly greater detail, as given in Figure 1.2(b). In this case the information source provides an electrical signal to a transmitter comprising an electrical stage which drives an optical source to give modulation of the lightwave carrier. The optical source which provides the electrical-optical conversion may be either a semiconductor laser or light-emitting diode (LED). The transmission medium consists of an optical fiber cable and the receiver consists of an optical detector which drives a further electrical stage and hence provides demodulation of the optical carrier. Photodiodes (*p-n*, *p-i-n* or avalanche) and, in some instances, phototransistors and photoconductors are utilized for the detection of the optical signal and the optical-electrical conversion. Thus there is a requirement for electrical interfacing at either end of the optical link and at present the signal processing is usually performed electrically.*

The optical carrier may be modulated using either an analog or digital information signal. In the system shown in Figure 1.2(b) analog modulation involves the variation of the light emitted from the optical source in a continuous manner. With digital modulation, however, discrete changes in the light intensity are obtained (i.e. on-off pulses). Although often simpler to implement, analog modulation with an optical fiber communication system is less efficient, requiring a far higher signal-to-noise ratio at the receiver than digital modulation. Also, the linearity needed for analog modulation is not always provided by semiconductor optical sources, especially at high modulation frequencies. For these reasons, analog optical fiber communication links are generally limited to shorter distances and lower bandwidth operation than digital links.

* Significant developments have taken place in devices for optical signal processing which are starting to alter this situation (see Chapter 11).

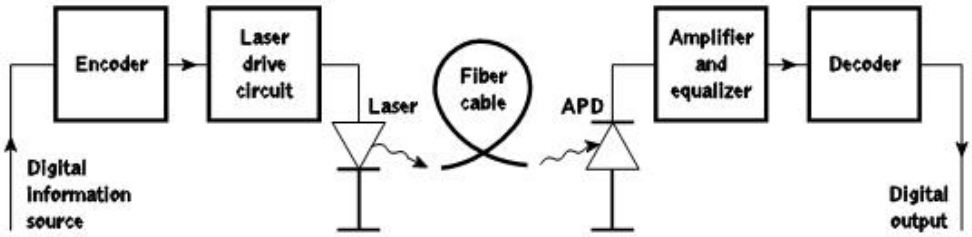

Figure 1.3 A digital optical fiber link using a semiconductor laser source and an avalanche photodiode (APD) detector

Figure 1.3 shows a block schematic of a typical digital optical fiber link. Initially, the input digital signal from the information source is suitably encoded for optical transmission. The laser drive circuit directly modulates the intensity of the semiconductor laser with the encoded digital signal. Hence a digital optical signal is launched into the optical fiber cable. The avalanche photodiode (APD) detector is followed by a front-end amplifier and equalizer or filter to provide gain as well as linear signal processing and noise bandwidth reduction. Finally, the signal obtained is decoded to give the original digital information. The various elements of this and alternative optical fiber system configurations are discussed in detail in the following chapters. However, at this stage it is instructive to consider the advantages provided by lightwave communication via optical fibers in comparison with other forms of line and radio communication which have brought about the extensive use of such systems in many areas throughout the world.

1.3 Advantages of optical fiber communication

Communication using an optical carrier wave guided along a glass fiber has a number of extremely attractive features, several of which were apparent when the technique was originally conceived. Furthermore, the advances in the technology to date have surpassed even the most optimistic predictions, creating additional advantages. Hence it is useful to consider the merits and special features offered by optical fiber communications over more conventional electrical communications. In this context we commence with the originally foreseen advantages and then consider additional features which have become apparent as the technology has been developed.

(a) Enormous potential bandwidth. The optical carrier frequency in the range 10^{13} to 10^{16} Hz (generally in the near infrared around 10^{14} Hz or 10^{5} GHz) yields a far greater potential transmission bandwidth than metallic cable systems (i.e. coaxial cable bandwidth typically around 20 MHz over distances up to a maximum of 10 km) or even millimeter wave radio systems (i.e. systems currently operating with modulation bandwidths of 700 MHz over a few hundreds of meters). Indeed, by the year 2000 the typical bandwidth multiplied by length product for an optical fiber link incorporating fiber amplifiers (see Section 10.4) was 5000 GHz km in comparison with the typical bandwidth-length product for coaxial cable of around 100 MHz km. Hence at this time optical fiber was already

demonstrating a factor of 50 000 bandwidth improvement over coaxial cable while also providing this superior information-carrying capacity over much longer transmission distances [Ref. 16].

Although the usable fiber bandwidth will be extended further towards the optical carrier frequency, it is clear that this parameter is limited by the use of a single optical carrier signal. Hence a much enhanced bandwidth utilization for an optical fiber can be achieved by transmitting several optical signals, each at different center wavelengths, in parallel on the same fiber. This wavelength division multiplexed operation (see Section 12.9.4), particularly with dense packing of the optical wavelengths (or, essentially, fine frequency spacing), offers the potential for a fiber information-carrying capacity that is many orders of magnitude in excess of that obtained using copper cables or a wideband radio system.

(b) Small size and weight. Optical fibers have very small diameters which are often no greater than the diameter of a human hair. Hence, even when such fibers are covered with protective coatings they are far smaller and much lighter than corresponding copper cables. This is a tremendous boon towards the alleviation of duct congestion in cities, as well as allowing for an expansion of signal transmission within mobiles such as aircraft, satellites and even ships.

(c) Electrical isolation. Optical fibers which are fabricated from glass, or sometimes a plastic polymer, are electrical insulators and therefore, unlike their metallic counterparts, they do not exhibit earth loop and interface problems. Furthermore, this property makes optical fiber transmission ideally suited for communication in electrically hazardous environments as the fibers create no arcing or spark hazard at abrasions or short circuits.

(d) Immunity to interference and crosstalk. Optical fibers form a dielectric waveguide and are therefore free from electromagnetic interference (EMI), radio-frequency interference (RFI), or switching transients giving electromagnetic pulses (EMPs). Hence the operation of an optical fiber communication system is unaffected by transmission through an electrically noisy environment and the fiber cable requires no shielding from EMI. The fiber cable is also not susceptible to lightning strikes if used overhead rather than underground. Moreover, it is fairly easy to ensure that there is no optical interference between fibers and hence, unlike communication using electrical conductors, crosstalk is negligible, even when many fibers are cabled together.

(e) Signal security. The light from optical fibers does not radiate significantly and therefore they provide a high degree of signal security. Unlike the situation with copper cables, a transmitted optical signal cannot be obtained from a fiber in a noninvasive manner (i.e. without drawing optical power from the fiber). Therefore, in theory, any attempt to acquire a message signal transmitted optically may be detected. This feature is obviously attractive for military, banking and general data transmission (i.e. computer network) applications.

(f) Low transmission loss. The development of optical fibers over the last 20 years has resulted in the production of optical fiber cables which exhibit very low attenuation or transmission loss in comparison with the best copper conductors. Fibers have been

fabricated with losses as low as 0.15 dB km^{-1} (see Section 3.3.2) and this feature has become a major advantage of optical fiber communications. It facilitates the implementation of communication links with extremely wide optical repeater or amplifier spacings, thus reducing both system cost and complexity. Together with the already proven modulation bandwidth capability of fiber cables, this property has provided a totally compelling case for the adoption of optical fiber communications in the majority of long-haul telecommunication applications, replacing not only copper cables, but also satellite communications, as a consequence of the very noticeable delay incurred for voice transmission when using this latter approach.

(g) Ruggedness and flexibility. Although protective coatings are essential, optical fibers may be manufactured with very high tensile strengths (see Section 4.6). Perhaps surprisingly for a glassy substance, the fibers may also be bent to quite small radii or twisted without damage. Furthermore, cable structures have been developed (see Section 4.8.4) which have proved flexible, compact and extremely rugged. Taking the size and weight advantage into account, these optical fiber cables are generally superior in terms of storage, transportation, handling and installation to corresponding copper cables, while exhibiting at least comparable strength and durability.

(h) System reliability and ease of maintenance. These features primarily stem from the low-loss property of optical fiber cables which reduces the requirement for intermediate repeaters or line amplifiers to boost the transmitted signal strength. Hence with fewer optical repeaters or amplifiers, system reliability is generally enhanced in comparison with conventional electrical conductor systems. Furthermore, the reliability of the optical components is no longer a problem with predicted lifetimes of 20 to 30 years being quite common. Both these factors also tend to reduce maintenance time and costs.

(i) Potential low cost. The glass which generally provides the optical fiber transmission medium is made from sand - not a scarce resource. So, in comparison with copper conductors, optical fibers offer the potential for low-cost line communication. Although over recent years this potential has largely been realized in the costs of the optical fiber transmission medium which for bulk purchases has become competitive with copper wires (i.e. twisted pairs), it has not yet been achieved in all the other component areas associated with optical fiber communications. For example, the costs of high-performance semiconductor lasers and detector photodiodes are still relatively high, as well as some of those concerned with the connection technology (demountable connectors, couplers, etc.).

Overall system costs when utilizing optical fiber communication on long-haul links, however, are substantially less than those for equivalent electrical line systems because of the low-loss and wideband properties of the optical transmission medium. As indicated in (f), the requirement for intermediate repeaters and the associated electronics is reduced, giving a substantial cost advantage. Although this cost benefit gives a net gain for longhaul links, it is not always the case in short-haul applications where the additional cost incurred, due to the electrical-optical conversion (and vice versa), may be a deciding factor. Nevertheless, there are other possible cost advantages in relation to shipping, handling, installation and maintenance, as well as the features indicated in (c) and (d) which may prove significant in the system choice.

The reducing costs of optical fiber communications has provided strong competition not only with electrical line transmission systems, but also for microwave and millimeter wave radio transmission systems. Although these systems are reasonably wideband, the relatively short-span 'line of sight' transmission necessitates expensive aerial towers at intervals no greater than a few tens of kilometers. Hence, with the exception of the telecommunication access network (see Section 15.6.3) due primarily to current first installed cost constraints, optical fiber has become the dominant transmission medium within the major industrialized societies.

Many advantages are therefore provided by the use of a lightwave carrier within a transmission medium consisting of an optical fiber. The fundamental principles giving rise to these enhanced performance characteristics, together with their practical realization, are described in the following chapters. However, a general understanding of the basic nature and properties of light is assumed. If this is lacking, the reader is directed to the many excellent texts encompassing the topic, a few of which are indicated in Refs 19 to 23.

CHAPTER 2

Optical fiber waveguides

2.1 Introduction

The transmission of light via a dielectric waveguide structure was first proposed and investigated at the beginning of the twentieth century. In 1910 Hondros and Debye [Ref. 1] conducted a theoretical study, and experimental work was reported by Schriever in 1920 [Ref. 2]. However, a transparent dielectric rod, typically of silica glass with a refractive index of around 1.5, surrounded by air, proved to be an impractical waveguide due to its unsupported structure (especially when very thin waveguides were considered in order to limit the number of optical modes propagated) and the excessive losses at any discontinuities of the glass-air interface. Nevertheless, interest in the application of dielectric optical waveguides in such areas as optical imaging and medical diagnosis (e.g. endoscopes) led to proposals [Refs 3, 4] for a clad dielectric rod in the mid-1950s in order to overcome these problems. This structure is illustrated in Figure 2.1, which shows a transparent core with a refractive index n_1 surrounded by a transparent cladding of slightly lower refractive index n_2. The cladding supports the waveguide structure while also, when

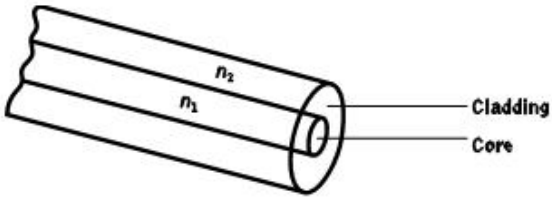

Figure 2.1 Optical fiber waveguide showing the core of refractive index n_1, surrounded by the cladding of slightly lower refractive index n_2

sufficiently thick, substantially reducing the radiation loss into the surrounding air. In essence, the light energy travels in both the core and the cladding allowing the associated fields to decay to a negligible value at the cladding-air interface.

The invention of the clad waveguide structure led to the first serious proposals by Kao and Hockham [Ref. 5] and Werts [Ref. 6], in 1966, to utilize optical fibers as a communications medium, even though they had losses in excess of 1000 dB km^{-1}. These proposals stimulated tremendous efforts to reduce the attenuation by purification of the materials. This has resulted in improved conventional glass refining techniques giving fibers with losses of around 4.2 dB km^{-1} [Ref. 7]. Also, progress in glass refining processes such as depositing vapor-phase reagents to form silica [Ref. 8] allowed fibers with losses below 1 dB km^{-1} to be fabricated.

Most of this work was focused on the 0.8 to 0.9 μm wavelength band because the first generation of optical sources fabricated from gallium aluminum arsenide alloys operated in this region. However, as silica fibers were studied in further detail it became apparent that transmission at longer wavelengths (1.1 to 1.6 μm) would result in lower losses and reduced signal dispersion. This produced a shift in optical fiber source and detector technology in order to provide operation at these longer wavelengths. Hence at longer wavelengths, especially around 1.55 μm, typical high-performance fibers have losses of 0.2 dB km^{-1} [Ref. 9].

As such losses are very close to the theoretical lower limit for silicate glass fiber, there is interest in glass-forming systems which can provide low-loss transmission in the mid-infrared (2 to 5 μm) optical wavelength regions. Although a system based on fluoride glass offers the potential for ultra-low-loss transmission of 0.01 dB km^{-1} at a wavelength of 2.55 μm, such fibers still exhibit losses of at least 0.65 dB km^{-1} and they also cannot yet be produced with the robust mechanical properties of silica fibers [Ref. 10].

In order to appreciate the transmission mechanism of optical fibers with dimensions approximating to those of a human hair, it is necessary to consider the optical waveguiding of a cylindrical glass fiber. Such a fiber acts as an open optical waveguide, which may be analyzed utilizing simple ray theory. However, the concepts of geometric optics are not sufficient when considering all types of optical fiber, and electromagnetic mode theory must be used to give a complete picture. The following sections will therefore outline the transmission of light in optical fibers prior to a more detailed discussion of the various types of fiber.

In Section 2.2 we continue the discussion of light propagation in optical fibers using the ray theory approach in order to develop some of the fundamental parameters associated with optical fiber transmission (acceptance angle, numerical aperture, etc.). Furthermore,

this provides a basis for the discussion of electromagnetic wave propagation presented in Section 2.3, where the electromagnetic mode theory is developed for the planar (rectangular) waveguide. Then, in Section 2.4, we discuss the waveguiding mechanism within cylindrical fibers prior to consideration of both step and graded index fibers. Finally, in Section 2.5 the theoretical concepts and important parameters (cutoff wavelength, spot size, propagation constant, etc.) associated with optical propagation in single-mode fibers are introduced and approximate techniques to obtain values for these parameters are described.

All consideration in the above sections is concerned with what can be referred to as conventional optical fiber in the context that it comprises both solid-core and cladding regions as depicted in Figure 2.1. In the mid-1990s, however, a new class of microstructured optical fiber, termed photonic crystal fiber, was experimentally demonstrated [Ref. 11] which has subsequently exhibited the potential to deliver applications ranging from light transmission over distance to optical device implementations (e.g. power splitters, amplifiers, bistable switches, wavelength converters). The significant physical feature of this microstructured optical fiber is that it typically contains an array of air holes running along the longitudinal axis rather than consisting of a solid silica rod structure. Moreover, the presence of these holes provides an additional dimension to fiber design which has already resulted in new developments for both guiding and controlling light. Hence the major photonic crystal fiber structures and their guidance mechanisms are outlined and discussed in Section 2.6 in order to give an insight into the fundamental developments of this increasingly important fiber class.

2.2 Ray theory transmission

2.2.1 Total internal reflection

To consider the propagation of light within an optical fiber utilizing the ray theory model it is necessary to take account of the refractive index of the dielectric medium. The refractive index of a medium is defined as the ratio of the velocity of light in a vacuum to the velocity of light in the medium. A ray of light travels more slowly in an optically dense medium than in one that is less dense, and the refractive index gives a measure of this effect. When a ray is incident on the interface between two dielectrics of differing refractive indices (e.g. glass-air), refraction occurs, as illustrated in Figure 2.2(a). It may be observed that the ray approaching the interface is propagating in a dielectric of refractive index n_1 and is at an angle φ_1 to the normal at the surface of the interface. If the dielectric on the other side of the interface has a refractive index n_2 which is less than n_1, then the refraction is such that the ray path in this lower index medium is at an angle φ_2 to the normal, where φ_2 is greater than φ_1. The angles of incidence φ_1 and refraction φ_2 are related to each other and to the refractive indices of the dielectrics by Snell's law of refraction [Ref. 12], which states that:

$$n_1 \sin \varphi_1 = n_2 \sin \varphi_2$$

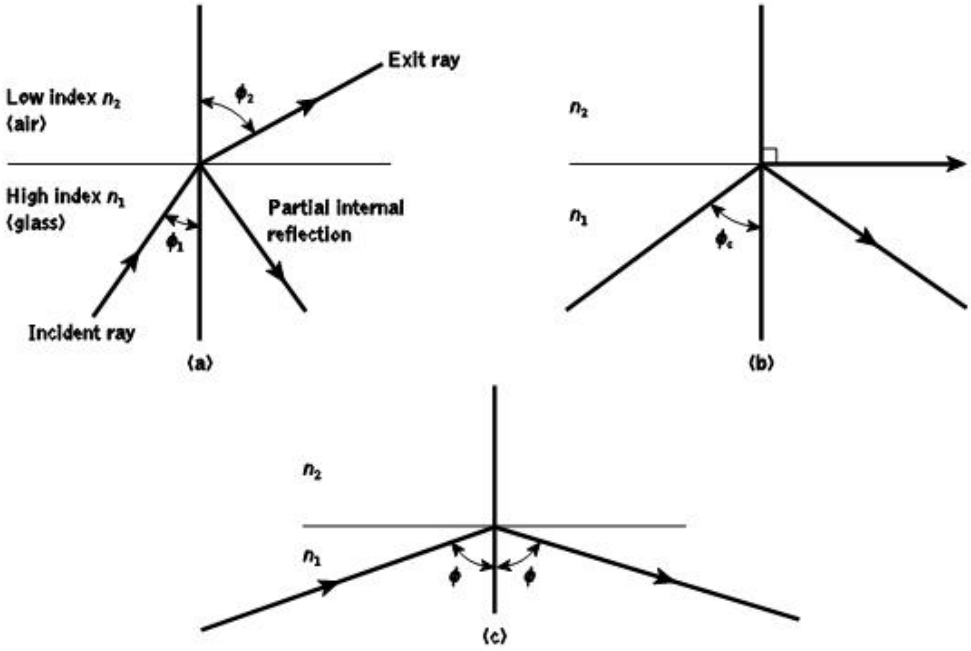

Figure 2.2 Light rays incident on a high to low refractive index interface (e.g. glass-air): (a) refraction; (b) the limiting case of refraction showing the critical ray at an angle φ_c; (c) total internal reflection where $\varphi > \varphi_c$

or:

$$\frac{\sin \varphi_1}{\sin \varphi_2} = \frac{n_2}{n_1} \tag{2.1}$$

It may also be observed in Figure 2.2(a) that a small amount of light is reflected back into the originating dielectric medium (partial internal reflection). As n_1 is greater than n_2, the angle of refraction is always greater than the angle of incidence. Thus when the angle of refraction is 90° and the refracted ray emerges parallel to the interface between the dielectrics, the angle of incidence must be less than 90°. This is the limiting case of refraction and the angle of incidence is now known as the critical angle φ_c, as shown in Figure 2.2(b). From Eq. (2.1) the value of the critical angle is given by:

$$\sin \varphi_c = \frac{n_2}{n_1} \tag{2.2}$$

At angles of incidence greater than the critical angle the light is reflected back into the originating dielectric medium (total internal reflection) with high efficiency (around 99.9%). Hence, it may be observed in Figure 2.2(c) that total internal reflection occurs at the interface between two dielectrics of differing refractive indices when light is incident on the dielectric of lower index from the dielectric of higher index, and the angle of incidence of

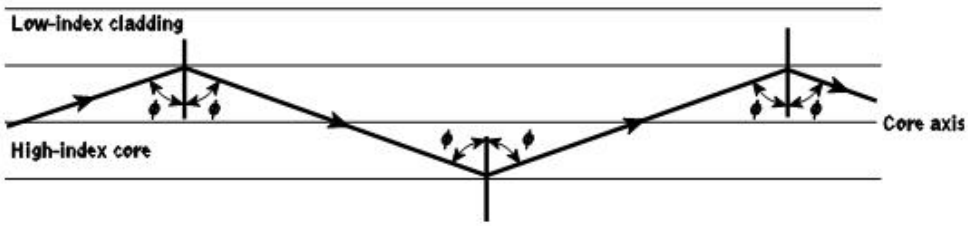

Figure 2.3 The transmission of a light ray in a perfect optical fiber

the ray exceeds the critical value. This is the mechanism by which light at a sufficiently shallow angle (less than $90° - \varphi_c$) may be considered to propagate down an optical fiber with low loss. Figure 2.3 illustrates the transmission of a light ray in an optical fiber via a series of total internal reflections at the interface of the silica core and the slightly lower refractive index silica cladding. The ray has an angle of incidence φ at the interface which is greater than the critical angle and is reflected at the same angle to the normal.

The light ray shown in Figure 2.3 is known as a meridional ray as it passes through the axis of the fiber core. This type of ray is the simplest to describe and is generally used when illustrating the fundamental transmission properties of optical fibers. It must also be noted that the light transmission illustrated in Figure 2.3 assumes a perfect fiber, and that any discontinuities or imperfections at the core-cladding interface would probably result in refraction rather than total internal reflection, with the subsequent loss of the light ray into the cladding.

2.2.2 Acceptance angle

Having considered the propagation of light in an optical fiber through total internal reflection at the core-cladding interface, it is useful to enlarge upon the geometric optics approach with reference to light rays entering the fiber. Since only rays with a sufficiently shallow grazing angle (i.e. with an angle to the normal greater than φ_c) at the core-cladding interface are transmitted by total internal reflection, it is clear that not all rays entering the fiber core will continue to be propagated down its length.

The geometry concerned with launching a light ray into an optical fiber is shown in Figure 2.4, which illustrates a meridional ray *A* at the critical angle φ_c within the fiber at the core-cladding interface. It may be observed that this ray enters the fiber core at an angle θ_a to the fiber axis and is refracted at the air-core interface before transmission to the core-cladding interface at the critical angle. Hence, any rays which are incident into the fiber core at an angle greater than θ_a will be transmitted to the core-cladding interface at an angle less than φ_c, and will not be totally internally reflected. This situation is also illustrated in Figure 2.4, where the incident ray *B* at an angle greater than θ_a is refracted into the cladding and eventually lost by radiation. Thus for rays to be transmitted by total internal reflection within the fiber core they must be incident on the fiber core within an acceptance cone defined by the conical half angle θ_a. Hence θ_a is the maximum angle to the axis at which light may enter the fiber in order to be propagated, and is often referred to as the acceptance angle* for the fiber.

* θ_a is sometimes referred to as the maximum or total acceptance angle.

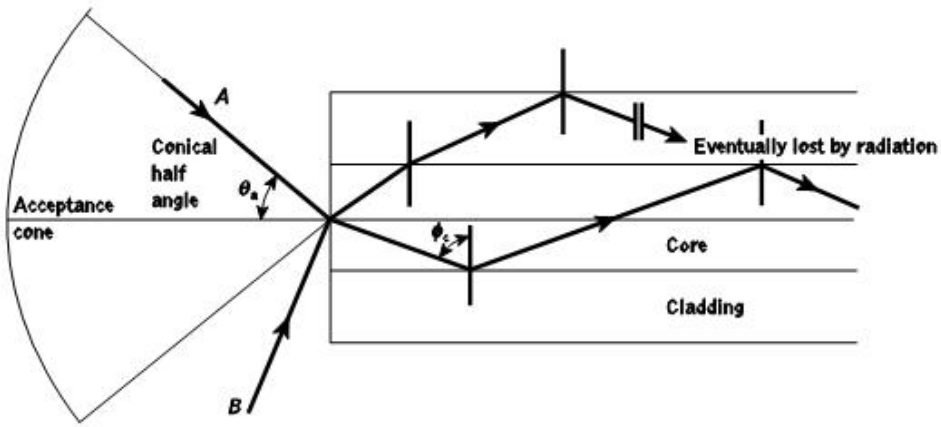

Figure 2.4 The acceptance angle θ_a when launching light into an optical fiber

If the fiber has a regular cross-section (i.e. the core-cladding interfaces are parallel and there are no discontinuities) an incident meridional ray at greater than the critical angle will continue to be reflected and will be transmitted through the fiber. From symmetry considerations it may be noted that the output angle to the axis will be equal to the input angle for the ray, assuming the ray emerges into a medium of the same refractive index from which it was input.

2.2.3 Numerical aperture

The acceptance angle for an optical fiber was defined in the preceding section. However, it is possible to continue the ray theory analysis to obtain a relationship between the acceptance angle and the refractive indices of the three media involved, namely the core, cladding and air. This leads to the definition of a more generally used term, the numerical aperture of the fiber. It must be noted that within this analysis, as with the preceding discussion of acceptance angle, we are concerned with meridional rays within the fiber.

Figure 2.5 shows a light ray incident on the fiber core at an angle θ_1 to the fiber axis which is less than the acceptance angle for the fiber θ_a. The ray enters the fiber from a

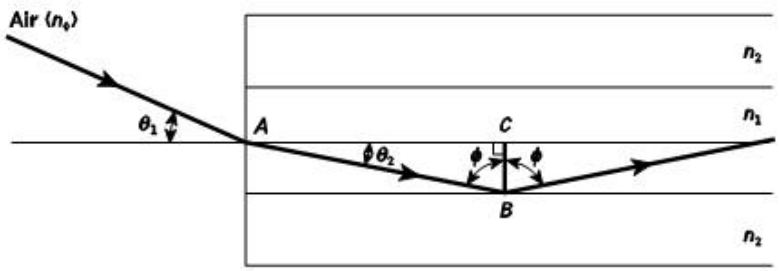

Figure 2.5 The ray path for a meridional ray launched into an optical fiber in air at an input angle less than the acceptance angle for the fiber

medium (air) of refractive index n_0, and the fiber core has a refractive index n_1, which is slightly greater than the cladding refractive index n_2. Assuming the entrance face at the fiber core to be normal to the axis, then considering the refraction at the air-core interface and using Snell's law given by Eq. (2.1):

$$n_0 \sin \theta_1 = n_1 \sin \theta_2 \tag{2.3}$$

Considering the right-angled triangle *ABC* indicated in Figure 2.5, then:

$$\varphi = \frac{\pi}{2} - \theta_2 \tag{2.4}$$

where φ is greater than the critical angle at the core-cladding interface. Hence Eq. (2.3) becomes:

$$n_0 \sin \theta_1 = n_1 \cos \varphi \tag{2.5}$$

Using the trigonometrical relationship $\sin^2 \varphi + \cos^2 \varphi = 1$, Eq. (2.5) may be written in the form:

$$n_0 \sin \theta_1 = n_1 (1 - \sin^2 \varphi)^{1/2} \tag{2.6}$$

When the limiting case for total internal reflection is considered, φ becomes equal to the critical angle for the core-cladding interface and is given by Eq. (2.2). Also in this limiting case θ_1 becomes the acceptance angle for the fiber θ_a. Combining these limiting cases into Eq. (2.6) gives:

$$n_0 \sin \theta_a = (n_1^2 - n_2^2)^{1/2} \tag{2.7}$$

Equation (2.7), apart from relating the acceptance angle to the refractive indices, serves as the basis for the definition of the important optical fiber parameter, the numerical aperture (*NA*). Hence the *NA* is defined as:

$$NA = n_0 \sin \theta_a = (n_1^2 - n_2^2)^{1/2} \tag{2.8}$$

Since the *NA* is often used with the fiber in air where n_0 is unity, it is simply equal to $\sin \theta_a$. It may also be noted that incident meridional rays over the range $0 \leq \theta_1 \leq \theta_a$ will be propagated within the fiber.

The *NA* may also be given in terms of the relative refractive index difference Δ between the core and the cladding which is defined as:*

* Sometimes another parameter $\Delta n = n_1 - n_2$ is referred to as the index difference and $\Delta n/n_1$ as the fractional index difference. Hence Δ also approximates to the fractional index difference.

$$\Delta = \frac{n^1 - n^2}{2n^1}$$

$$\frac{n_1 - n_2}{n_1} \quad \text{for } \Delta \quad 1 \tag{2.9}$$

Hence combining Eq. (2.8) with Eq. (2.9) we can write:

$$NA = n_1(2\Delta)^{\leftarrow 2} \tag{2.10}$$

The relationships given in Eqs (2.8) and (2.10) for the numerical aperture are a very useful measure of the light-collecting ability of a fiber. They are independent of the fiber core diameter and will hold for diameters as small as 8 μm. However, for smaller diameters they break down as the geometric optics approach is invalid. This is because the ray theory model is only a partial description of the character of light. It describes the direction a plane wave component takes in the fiber but does not take into account interference between such components. When interference phenomena are considered it is found that only rays with certain discrete characteristics propagate in the fiber core. Thus the fiber will only support a discrete number of guided modes. This becomes critical in smallcore-diameter fibers which only support one or a few modes. Hence electromagnetic mode theory must be applied in these cases (see Section 2.3).

Example 2.1

A silica optical fiber with a core diameter large enough to be considered by ray theory analysis has a core refractive index of 1.50 and a cladding refractive index of 1.47.

Determine: (a) the critical angle at the core-cladding interface; (b) the *NA* for the fiber; (c) the acceptance angle in air for the fiber.

Solution: (a) The critical angle φ_c at the core-cladding interface is given by Eq. (2.2) where:

$$\varphi_c = \sin_{-1} \frac{n_2}{n_1} = \sin^{-1} \frac{1.47}{1.50}$$
$$= 78.5°$$

(b) From Eq. (2.8) the *NA* is:

$$NA = (n_2 - n_2)^{\overline{\varphi}} = (1.50^2 - 1.47^2)^{\overline{\imath}^{-2}}$$
$$= (2.25 - 2.16)^{\overline{\imath}^{-2}}$$
$$= 0.30$$

(c) Considering Eq. (2.8) the acceptance angle in air θ_a is given by: $\theta_a =$

$\sin_{-1} NA = \sin^{-1} 0.30$
$= 17.4°$

Example 2.2

A typical relative refractive index difference for an optical fiber designed for longdistance transmission is 1%. Estimate the *NA* and the solid acceptance angle in air for the fiber when the core index is 1.46. Further, calculate the critical angle at the core-cladding interface within the fiber. It may be assumed that the concepts of geometric optics hold for the fiber.

Solution: Using Eq. (2.10) with $\Delta = 0.01$ gives the *NA* as:

$$NA = n_1(2\Delta)^{\frac{1}{2}} = 1.46(0.02)^{\frac{1}{2}}$$
$$= 0.21$$

For small angles the solid acceptance angle in air ζ is given by:

$$\zeta \quad \pi\theta_2 = \pi \sin^2 \theta_a$$

Hence from Eq. (2.8):

$$\zeta \quad \pi (NA)^2 = \pi \times 0.04$$
$$= 0.13 \text{ rad}$$

Using Eq. (2.9) for the relative refractive index difference Δ gives:

$$\Delta \quad \frac{n_1 - n_2}{n_1} = 1 - \frac{n_2}{n_1}$$

Hence

$$\frac{n_2}{n_1} = 1 - \Delta = 1 - 0.01$$
$$= 0.99$$

From Eq. (2.2) the critical angle at the core-cladding interface is:

$$\varphi_c = \sin^{-1} \frac{n_2}{n_1} = \sin^{-1} 0.99$$
$$= 81.9°$$

CHAPTER 3

Transmission characteristics of optical fibers

3.1 Introduction

The basic transmission mechanisms of the various types of optical fiber waveguide have been discussed in Chapter 2. However, the factors which affect the performance of optical fibers as a transmission medium were not dealt with in detail. These transmission characteristics are of utmost importance when the suitability of optical fibers for communication purposes is investigated. The transmission characteristics of most interest are those of attenuation (or loss) and bandwidth.

The huge potential bandwidth of optical communications helped stimulate the birth of the idea that a dielectric waveguide made of glass could be used to carry wideband telecommunication signals. This occurred, as indicated in Section 2.1 in the celebrated papers by Kao and Hockham, and Werts, in 1966. However, at the time the idea may have seemed somewhat ludicrous as a typical block of glass could support optical transmission for at best a few tens of meters before it was attenuated to an unacceptable level. Nevertheless, careful investigation of the attenuation showed that it was largely due to absorption in the glass, caused by impurities such as iron, copper, manganese and other transition metals which occur in the third row of the periodic table. Hence, research was stimulated towards a new generation of 'pure' glasses for use in optical fiber communications.

A major breakthrough came in 1970 when the first fiber with an attenuation below 20 dB km^{-1} was reported [Ref. 1]. This level of attenuation was seen as the absolute minimum that had to be achieved before an optical fiber system could in any way compete economically with existing communication systems. Since 1970 tremendous improvements have been made, leading to silica-based glass fibers with losses of less than 0.2 dB km^{-1} in the laboratory by the late 1980s [Ref. 2]. Hence, comparatively low-loss fibers have been incorporated into optical communication systems throughout the world. Although the fundamental lower limits for attenuation in silicate glass fibers were largely achieved by 1990, continuing significant progress has been made in relation to the removal of the water impurity peak within the operational wavelength range [Ref. 3]. The investigation of other material systems which can exhibit substantially lower losses when operated at longer wavelengths [Ref. 2] has, however, slowed down in relation to telecommunication transmission due to difficulties in the production of fiber with both optical and mechanical properties that will compete with silica. In particular, such mid-infrared (and possibly far-infrared) transmitting fibers continue to exhibit both relatively high losses and low strength [Ref. 4].

The other characteristic of primary importance is the bandwidth of the fiber. This is limited by the signal dispersion within the fiber, which determines the number of bits of information transmitted in a given time period. Therefore, once the attenuation was reduced to acceptable levels, attention was directed towards the dispersive properties of fibers Again, this has led to substantial improvements, giving wideband fiber bandwidths of many tens of gigahertz over a number of kilometers.

In order to appreciate these advances and possible future developments, the optical transmission characteristics of fibers must be considered in greater depth. Therefore, in this chapter we discuss the mechanisms within optical fibers which give rise to the major transmission characteristics mentioned previously (attenuation and dispersion), while also considering other, perhaps less obvious, effects when light is propagating down an optical fiber (modal noise, polarization and nonlinear phenomena).

We begin the discussion of attenuation in Section 3.2 with calculation of the total losses incurred in optical fibers. The various attenuation mechanisms (material absorption, linear scattering, nonlinear scattering, fiber bends) are then considered in detail in Sections 3.3 to 3.6. The primary focus within these sections is on silica-based glass fibers. However, in Section 3.7 consideration is given to other material systems which are employed for mid-infrared and far-infrared optical transmission. Dispersion in optical fibers is described in Section 3.8, together with the associated limitations on fiber bandwidth. Sections 3.9 and 3.10 deal with chromatic (intramodal) and intermodal dispersion mechanisms and included in the latter section is a discussion of the modal noise phenomenon associated with intermodal dispersion. Overall signal dispersion in both multimode and single-mode fibers is then considered in Section 3.11. This is followed in Section 3.12 by a review of the modification of the dispersion characteristics within single-mode fibers in order to obtain dispersion-shifted, dispersion-flattened and nonzero-dispersion-shifted fibers. Section 3.13 presents an account of the polarization within single-mode fibers which includes discussion of both polarization mode dispersion and the salient features of polarization-maintaining fibers. Nonlinear optical effects, which can occur at relatively high optical power levels within single-mode fibers, are then dealt with in Section 3.14 prior to a final Section 3.15 describing the special case of nonlinear pulse propagation referred to as soliton propagation.

3.2 Attenuation

The attenuation or transmission loss of optical fibers has proved to be one of the most important factors in bringing about their wide acceptance in telecommunications. As channel attenuation largely determined the maximum transmission distance prior to signal restoration, optical fiber communications became especially attractive when the transmission losses of fibers were reduced below those of the competing metallic conductors (less than 5 dB km^{-1}).

Signal attenuation within optical fibers, as with metallic conductors, is usually expressed in the logarithmic unit of the decibel. The decibel, which is used for comparing two power levels, may be defined for a particular optical wavelength as the ratio of the input (transmitted) optical power P_i into a fiber to the output (received) optical power P_o from the fiber as:

$$\text{Number of decibels (dB)} = 10 \log_{10} \frac{P_i}{P_o} \tag{3.1}$$

This logarithmic unit has the advantage that the operations of multiplication and division reduce to addition and subtraction, while powers and roots reduce to multiplication and division. However, addition and subtraction require a conversion to numerical values which may be obtained using the relationship:

$$\frac{P_i}{P_o} = 10^{(\text{dB}/10)} \tag{3.2}$$

In optical fiber communications the attenuation is usually expressed in decibels per unit length (i.e. dB km^{-1}) following:

$$\alpha_{dB}^{L} = 10 \log_{10} \frac{P_i}{P_o} \tag{3.3}$$

where α_{dB} is the signal attenuation per unit length in decibels which is also referred to as the fiber loss parameter and L is the fiber length.

Example 3.1

When the mean optical power launched into an 8 km length of fiber is 120 μW, the mean optical power at the fiber output is 3 μW.

Determine:

(a) the overall signal attenuation or loss in decibels through the fiber assuming there are no connectors or splices;

(b) the signal attenuation per kilometer for the fiber.

(c) the overall signal attenuation for a 10 km optical link using the same fiber with splices at 1 km intervals, each giving an attenuation of 1 dB;

(d) the numerical input/output power ratio in (c).

Solution: (a) Using Eq. (3.1), the overall signal attenuation in decibels through the fiber is:

$$\text{Signal attenuation} = 10 \log_{10} \frac{P_i}{P_o} = 10 \log_{10} \frac{120 \times 10^{-6}}{3 \times 10^{-6}}$$

$$= 10 \log_{10} 40 = 16.0 \text{ dB}$$

(b) The signal attenuation per kilometer for the fiber may be simply obtained by dividing the result in (a) by the fiber length which corresponds to it using Eq. (3.3) where:

$$\alpha_{dB}^{L} = 16.0 \text{ dB}$$

hence:

$$\alpha_{dB} = \frac{16.0}{8}$$

$$= 2.0 \text{ dB km}_{-1}$$

(c) As $\alpha_{dB} = 2$ dB km^{-1}, the loss incurred along 10 km of the fiber is given by: $\alpha_{dB} L =$

$2 \times 10 = 20$ dB

However, the link also has nine splices (at 1 km intervals) each with an attenuation of 1 dB. Therefore, the loss due to the splices is 9 dB.

Hence, the overall signal attenuation for the link is:

Signal attenuation = 20 + 9
= 29 dB

(d) To obtain a numerical value for the input/output power ratio, Eq. (3.2) may be used where:

$$\frac{P_i}{P_o} = 10^{29/10} = 794.3$$

A number of mechanisms are responsible for the signal attenuation within optical fibers. These mechanisms are influenced by the material composition, the preparation and purification technique, and the waveguide structure. They may be categorized within several major areas which include material absorption, material scattering (linear and nonlinear scattering), curve and microbending losses, mode coupling radiation losses and losses due to leaky modes. There are also losses at connectors and splices, as illustrated in Example 3.1. However, in this chapter we are interested solely in the characteristics of the fiber; connector and splice losses are dealt with in Section 5.2. It is instructive to consider in some detail the loss mechanisms within optical fibers in order to obtain an understanding of the problems associated with the design and fabrication of low-loss waveguides.

3.3 Material absorption losses in silica glass fibers

Material absorption is a loss mechanism related to the material composition and the fabrication process for the fiber, which results in the dissipation of some of the transmitted optical power as heat in the waveguide. The absorption of the light may be intrinsic (caused by the interaction with one or more of the major components of the glass) or extrinsic (caused by impurities within the glass).

3.3.1 Intrinsic absorption

An absolutely pure silicate glass has little intrinsic absorption due to its basic material structure in the near-infrared region. However, it does have two major intrinsic absorption

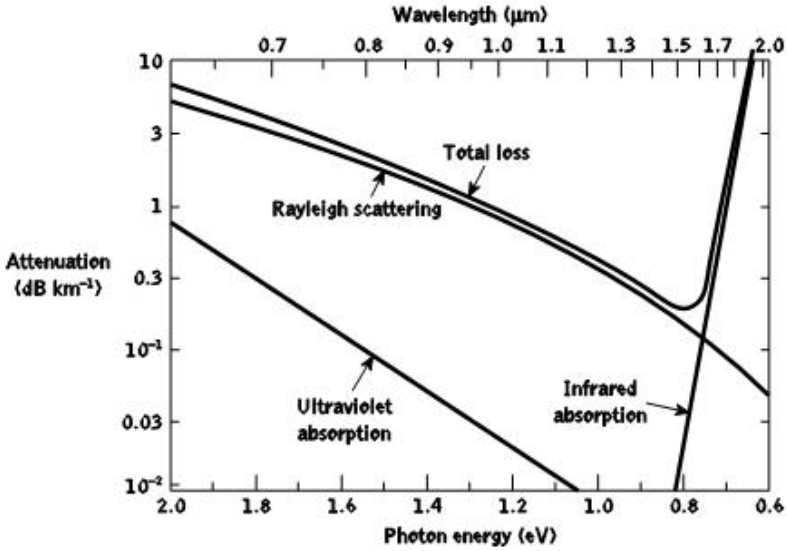

Figure 3.1 The attenuation spectra for the intrinsic loss mechanisms in pure GeO_2-SiO_2 glass [Ref. 5]

mechanisms at optical wavelengths which leave a low intrinsic absorption window over the 0.8 to 1.7 μm wavelength range, as illustrated in Figure 3.1, which shows a possible optical attenuation against wavelength characteristic for absolutely pure glass [Ref. 5]. It may be observed that there is a fundamental absorption edge, the peaks of which are centered in the ultraviolet wavelength region. This is due to the stimulation of electron transitions within the glass by higher energy excitations. The tail of this peak may extend into the window region at the shorter wavelengths, as illustrated in Figure 3.1. Also in the infrared and far infrared, normally at wavelengths above 7 μm, fundamentals of absorption bands from the interaction of photons with molecular vibrations within the glass occur. These give absorption peaks which again extend into the window region. The strong absorption bands occur due to oscillations of structural units such as Si-O (9.2 μm), P-O (8.1 μm), B-O (7.2 μm) and Ge-O (11.0 μm) within the glass. Hence, above 1.5 μm the tails of these largely far-infrared absorption peaks tend to cause most of the pure glass losses.

However, the effects of both these processes may be minimized by suitable choice of both core and cladding compositions. For instance, in some nonoxide glasses such as fluorides and chlorides, the infrared absorption peaks occur at much longer wavelengths which are well into the far infrared (up to 50 μm), giving less attenuation to longer wavelength transmission compared with oxide glasses.

3.3.2 Extrinsic absorption

In practical optical fibers prepared by conventional melting techniques (see Section 4.3), a major source of signal attenuation is extrinsic absorption from transition metal element impurities. Some of the more common metallic impurities found in glasses are shown in

Table 3.1 Absorption losses caused by some of the more common metallic ion impurities in glasses, together with the absorption peak wavelength

	Peak wavelength (nm)	*One part in 10^9 (dB km^{-1})*
Cr^{3+}	625	1.6
C^{2+}	685	0.1
Cu^{2+}	850	1.1
Fe^{2+}	1100	0.68
Fe^{3+}	400	0.15
Ni^{2+}	650	0.1
Mn^{3+}	460	0.2
V^{4+}	725	2.7

the Table 3.1, together with the absorption losses caused by one part in 10^9 [Ref. 6]. It may be noted that certain of these impurities, namely chromium and copper, in their worst valence state can cause attenuation in excess of 1 dB km^{-1} in the near-infrared region. Transition element contamination may be reduced to acceptable levels (i.e. one part in 10^{10}) by glass refining techniques such as vapor-phase oxidation [Ref. 7] (see Section 4.4), which largely eliminates the effects of these metallic impurities.

However, another major extrinsic loss mechanism is caused by absorption due to water (as the hydroxyl or OH ion) dissolved in the glass. These hydroxyl groups are bonded into the glass structure and have fundamental stretching vibrations which occur at wavelengths between 2.7 and 4.2 μm depending on group position in the glass network. The fundamental vibrations give rise to overtones appearing almost harmonically at 1.38, 0.95 and 0.72 μm, as illustrated in Figure 3.2. This shows the absorption spectrum for the hydroxyl

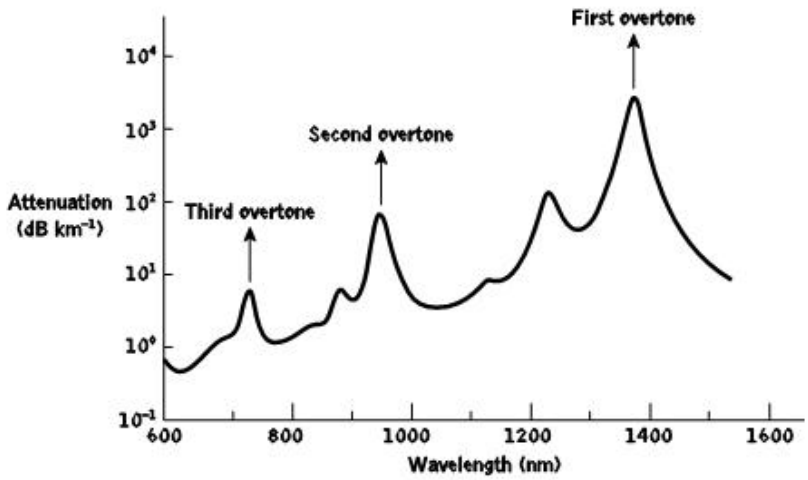

Figure 3.2 The absorption spectrum for the hydroxyl (OH) group in silica. Reproduced with permission from D. B. Keck, R. D. Maurer and P. C. Schultz, *Appl. Phys. Lett.*, **22**, p. 307, 1973. Copyright © 1973, American Institute of Physics

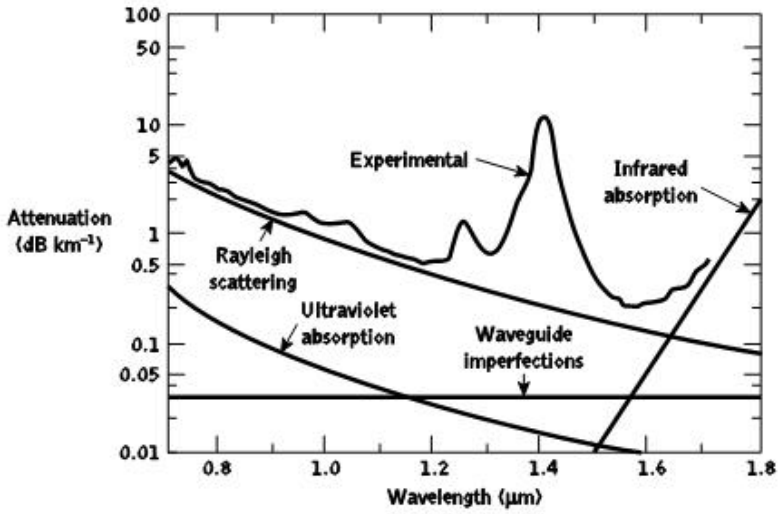

Figure 3.3 The measured attenuation spectrum for an ultra-low-loss single-mode fiber (solid line) with the calculated attenuation spectra for some of the loss mechanisms contributing to the overall fiber attenuation (dashed and dotted lines) [Ref. 5]

group in silica. Furthermore, combinations between the overtones and the fundamental SiO_2 vibration occur at 1.24, 1.13 and 0.88 μm, completing the absorption spectrum shown in Figure 3.2.

It may also be observed in Figure 3.2 that the only significant absorption band in the region below a wavelength of 1 μm is the second overtone at 0.95 μm which causes attenuation of about 1 dB km^{-1} for one part per million (ppm) of hydroxyl. At longer wavelengths the first overtone at 1.383 μm and its sideband at 1.24 μm are strong absorbers giving attenuation of about 2 dB km^{-1} ppm and 4 dB km^{-1} ppm respectively. Since most resonances are sharply peaked, narrow windows exist in the longer wavelength region around 1.31 and 1.55 μm which are essentially unaffected by OH absorption once the impurity level has been reduced below one part in 10^7. This situation is illustrated in Figure 3.3, which shows the attenuation spectrum of a low-loss single-mode fiber produced in 1979 [Ref. 5]. It may be observed that the lowest attenuation for this fiber occurs at a wavelength of 1.55 μm and is 0.2 dB km^{-1}. Despite this value approaching the minimum possible attenuation of around 0.18 dB km^{-1} at the 1.55 μm wavelength [Ref. 8], it should be noted that the transmission loss of an ultra-low-loss pure silica core fiber was more recently measured as 0.1484 dB km^{-1} at the slightly longer wavelength of 1.57 μm [Ref. 9].

Although in standard, modern single-mode fibers the loss caused by the primary OH peak at 1.383 μm has been reduced below 1 dB km^{-1}, it still limits operation over significant distances to the lower loss windows at 1.31 and 1.55 μm. A more recent major advance, however, has enabled the production of a revolutionary fiber type* in which the

* An example is the Alcatel-Lucent AllWave fiber which has typical losses of 0.32, 0.28 and 0.19 dB at wavelengths of 1.310, 1.383 and 1.550 μm, respectively. This fiber is referred to as exhibiting a zero water peak (ZWP) in the Alcatel-Lucent specification literature.

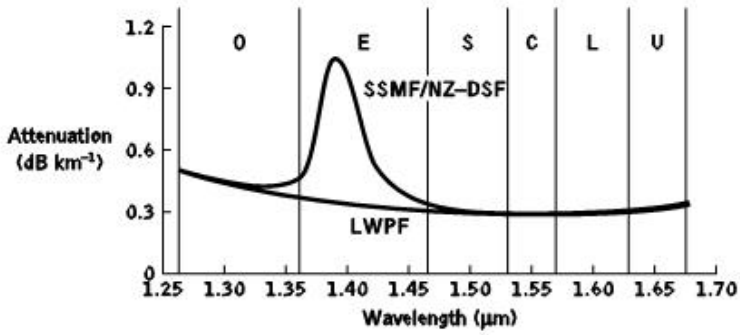

Figure 3.4 Fiber attenuation spectra: low-water-peak fiber compared with standard single-mode and nonzero-dispersion-shifted fibers

1.383 μm water peak has been permanently reduced to such levels that it is virtually eliminated [Ref. 10]. The attenuation spectrum for this low-water-peak fiber (LWPF), or dry fiber, is shown in Figure 3.4 where it is compared with standard single-mode fiber (SSMF) [Ref. 3].

The LWPF permits the transmission of optical signals over the full 1.260 to 1.675 μm wavelength range with losses less than 0.4 dB km^{-1} and therefore better facilitates wavelength division multiplexing (see Section 12.9.3). It may also be seen that the optical transmission wavelength band designations are also identified on the wavelength axis of Figure 3.4. These International Telecommunications Union (ITU) spectral band designations for both intermediate-range and long-distance optical fiber communications are indicated by the letters O, E, S, C, L and U, which are defined in Table 3.2 and are in common use in the field. It should be noted that long-haul transmission first took place in the O- and C-bands, subsequently followed by the L-band region. In addition, it is apparent that LWPF has enabled the use of the 1.460 to 1.530 μm window or S-band which is affected by the water peak in SSMF.

Table 3.2 ITU spectral band definitions

Name	*ITU band*	*Wavelength range (μm)*
Original band	O-band	1.260 to 1.360
Extended band	E-band	1.360 to 1.460
Short band	S-band	1.460 to 1.530
Conventional band	C-band	1.530 to 1.565
Long band	L-band	1.565 to 1.625
Ultralong band	U-band	1.625 to 1.675

3.4 Linear scattering losses

Linear scattering mechanisms cause the transfer of some or all of the optical power contained within one propagating mode to be transferred linearly (proportionally to the mode power) into a different mode. This process tends to result in attenuation of the transmitted light as the transfer may be to a leaky or radiation mode which does not continue to propagate within the fiber core, but is radiated from the fiber. It must be noted that as with all linear processes, there is no change of frequency on scattering.

Linear scattering may be categorized into two major types: Rayleigh and Mie scattering. Both result from the nonideal physical properties of the manufactured fiber which are difficult and, in certain cases, impossible to eradicate at present.

3.4.1 Rayleigh scattering

Rayleigh scattering is the dominant intrinsic loss mechanism in the low-absorption window between the ultraviolet and infrared absorption tails. It results from inhomogeneities of a random nature occurring on a small scale compared with the wavelength of the light. These inhomogeneities manifest themselves as refractive index fluctuations and arise from density and compositional variations which are frozen into the glass lattice on cooling. The compositional variations may be reduced by improved fabrication, but the index fluctuations caused by the freezing-in of density inhomogeneities are fundamental and cannot be avoided. The subsequent scattering due to the density fluctuations, which is in almost all directions, produces an attenuation proportional to $1/\lambda^4$ following the Rayleigh scattering formula [Ref. 11]. For a single-component glass this is given by:

$$\gamma_R = \frac{8\pi_3}{3\lambda^4} n^8 p^2 \beta_c K T_F \tag{3.4}$$

where γ_R is the Rayleigh scattering coefficient, λ is the optical wavelength, n is the refractive index of the medium, p is the average photoelastic coefficient, β_c is the isothermal compressibility at a fictive temperature T_F, and K is Boltzmann's constant. The fictive temperature is defined as the temperature at which the glass can reach a state of thermal equilibrium and is closely related to the anneal temperature. Furthermore, the Rayleigh scattering coefficient is related to the transmission loss factor (transmissivity) of the fiber following the relation [Ref. 12]:

$$= \exp(-\gamma_R L) \tag{3.5}$$

where L is the length of the fiber. It is apparent from Eq. (3.4) that the fundamental component of Rayleigh scattering is strongly reduced by operating at the longest possible wavelength. This point is illustrated in Example 3.2.

Example 3.2

Silica has an estimated fictive temperature of 1400 K with an isothermal compressibility of 7×10^{-11} m^2 N^{-1} [Ref. 13]. The refractive index and the photoelastic coefficient for silica are 1.46 and 0.286 respectively [Ref. 13]. Determine the theoretical attenuation in decibels per kilometer due to the fundamental Rayleigh scattering in silica at optical wavelengths of 0.63, 1.00 and 1.30 μm. Boltzmann's constant is 1.381×10^{-21} J K^{-1}.

Solution: The Rayleigh scattering coefficient may be obtained from Eq. (3.4) for each wavelength. However, the only variable in each case is the wavelength, and therefore the constant of proportionality of Eq. (3.4) applies in all cases. Hence:

$$\gamma_R = \frac{8\pi^3 n^8 p^2 \beta_c K T_F}{3\lambda^4}$$

$$= \frac{248.15 \times 20.65 \times 0.082 \times 7 \times 10^{-11} \times 1.381 \times 10^{-23} \times 1400}{3 \times \lambda^4}$$

$$= \frac{1.895 \times 10^{-28}}{\lambda^4} \text{ m}^{-1}$$

At a wavelength of 0.63 μm:

$$\gamma_R = \frac{1.895 \times 10^{-28}}{0.158 \times 10^{-24}} = 1.199 \times 10^{-3} \text{ m}^{-1}$$

The transmission loss factor for 1 kilometer of fiber may be obtained using Eq. (3.5):

$$\tau_{km} = \exp(-\gamma_R L) = \exp(-1.199 \times 10^{-3} \times 10^3)$$
$$= 0.301$$

The attenuation due to Rayleigh scattering in decibels per kilometer may be obtained from Eq. (3.1) where:

$$\text{Attenuation} = 10 \log_{10}(1/\tau_{km}) = 10 \log_{10} 3.322$$
$$= 5.2 \text{ dB km}^{-1}$$

At a wavelength of 1.0 μm:

$$\gamma_R = \frac{1.895 \times 10^{-28}}{10^{-24}} = 1.895 \times 10^{-4} \text{ m}^{-1}$$

Using Eq. (3.5):

$$\tau_{km} = \exp(-1.895 \times 10^{-4} \times 10^3) = \exp(-0.1895)$$
$$= 0.827$$

and Eq. (3.1):

Attenuation = $10 \log_{10} 1.209 = 0.8$ dB km^{-1} At

a wavelength of 1.30 μm:

$$\gamma_R = \frac{1.895 \times 10^{-28}}{2.856 \times 10^{-24}} = 0.664 \times 10^{-4}$$

Using Eq. (3.5):

$_{km} = \exp(-0.664 \times 10^{-4} \times 10^{3}) = 0.936$ and

Eq. (3.1):

Attenuation = $10 \log_{10} 1.069 = 0.3$ dB km^{-1}

The theoretical attenuation due to Rayleigh scattering in silica at wavelengths of 0.63, 1.00 and 1.30 μm, from Example 3.2, is 5.2, 0.8 and 0.3 dB km^{-1} respectively. These theoretical results are in reasonable agreement with experimental work. For instance, a low reported value for Rayleigh scattering in silica at a wavelength of 0.6328 μm is 3.9 dB km^{-1} [Ref. 13]. However, values of 4.8 dB km^{-1} [Ref. 14] and 5.4 dB km^{-1} [Ref. 15] have also been reported. The predicted attenuation due to Rayleigh scattering against wavelength is indicated by a dashed line on the attenuation characteristics shown in Figures 3.1 and 3.3.

3.4.2 Mie scattering

Linear scattering may also occur at inhomogeneities which are comparable in size with the guided wavelength. These result from the nonperfect cylindrical structure of the waveguide and may be caused by fiber imperfections such as irregularities in the core-cladding interface, core-cladding refractive index differences along the fiber length, diameter fluctuations, strains and bubbles. When the scattering inhomogeneity size is greater than $\lambda/10$, the scattered intensity which has an angular dependence can be very large.

The scattering created by such inhomogeneities is mainly in the forward direction and is called Mie scattering. Depending upon the fiber material, design and manufacture, Mie scattering can cause significant losses. The inhomogeneities may be reduced by:

(a) removing imperfections due to the glass manufacturing process;

(b) carefully controlled extrusion and coating of the fiber;

(c) increasing the fiber guidance by increasing the relative refractive index difference.

By these means it is possible to reduce Mie scattering to insignificant levels.

3.5 Nonlinear scattering losses

Optical waveguides do not always behave as completely linear channels whose increase in output optical power is directly proportional to the input optical power. Several nonlinear effects occur, which in the case of scattering cause disproportionate attenuation, usually at high optical power levels. This nonlinear scattering causes the optical power from one mode to be transferred in either the forward or backward direction to the same, or other modes, at a different frequency. It depends critically upon the optical power density within the fiber and hence only becomes significant above threshold power levels.

The most important types of nonlinear scattering within optical fibers are stimulated Brillouin and Raman scattering, both of which are usually only observed at high optical power densities in long single-mode fibers. These scattering mechanisms in fact give optical gain but with a shift in frequency, thus contributing to attenuation for light transmission at a specific wavelength. However, it may be noted that such nonlinear phenomena can also be used to give optical amplification in the context of integrated optical techniques (see Section 11.7). In addition, these nonlinear processes are explored in further detail both following and in Section 3.14.

3.5.1 Stimulated Brillouin scattering

Stimulated Brillouin scattering (SBS) may be regarded as the modulation of light through thermal molecular vibrations within the fiber. The scattered light appears as upper and lower sidebands which are separated from the incident light by the modulation frequency. The incident photon in this scattering process produces a phonon* of acoustic frequency as well as a scattered photon. This produces an optical frequency shift which varies with the scattering angle because the frequency of the sound wave varies with acoustic wavelength. The frequency shift is a maximum in the backward direction, reducing to zero in the forward direction, making SBS a mainly backward process.

As indicated previously, Brillouin scattering is only significant above a threshold power density. Assuming that the polarization state of the transmitted light is not maintained (see Section 3.12), it may be shown [Ref. 16] that the threshold power P_B is given by:

$$P_B = 4.4 \times 10^{-3} d^2 \lambda^2 \alpha_{dB} \nu \text{ watts} \tag{3.6}$$

where

d and λ are the fiber core diameter and the operating wavelength, respectively, both measured in micrometers, α_{dB} is the fiber attenuation in decibels per kilometer and ν is the source bandwidth (i.e. injection laser) in gigahertz. The expression given in Eq. (3.6) allows the determination of the threshold optical power which must be launched into a single-mode optical fiber before SBS occurs (see Example 3.3).

* The phonon is a quantum of an elastic wave in a crystal lattice. When the elastic wave has a frequency *f*, the quantized unit of the phonon has energy *hf* joules, where *h* is Planck's constant.

3.5.2 Stimulated Raman scattering

Stimulated Raman scattering (SRS) is similar to SBS except that a high-frequency optical phonon rather than an acoustic phonon is generated in the scattering process. Also, SRS can occur in both the forward and backward directions in an optical fiber, and may have an optical power threshold of up to three orders of magnitude higher than the Brillouin threshold in a particular fiber.

Using the same criteria as those specified for the Brillouin scattering threshold given in Eq. (3.6), it may be shown [Ref. 16] that the threshold optical power for SRS P_R in a long single-mode fiber is given by:

$$P_R = 5.9 \times 10^{-2} d^2 \lambda \alpha_{dB} \text{ watts} \tag{3.7}$$

where d, λ and α_{dB} are as specified for Eq. (3.6).

Example 3.3

A long single-mode optical fiber has an attenuation of 0.5 dB km^{-1} when operating at a wavelength of 1.3 μm. The fiber core diameter is 6 μm and the laser source bandwidth is 600 MHz. Compare the threshold optical powers for stimulated Brillouin and Raman scattering within the fiber at the wavelength specified.

Solution: The threshold optical power for SBS is given by Eq. (3.6) as:

$$P_B = 4.4 \times 10^{-3} d^2 \lambda^2 \alpha_{dB} \nu$$
$$= 4.4 \times 10^{-3} \times 6^2 \times 1.3^2 \times 0.5 \times 0.6 =$$
$$80.3 \text{ mW}$$

The threshold optical power for SRS may be obtained from Eq. (3.7), where:

$$P_R = 5.9 \times 10^{-2} d^2 \lambda \alpha_{dB}$$
$$= 5.9 \times 10^{-2} \times 6^2 \times 1.3 \times 0.5$$
$$= 1.38 \text{ W}$$

In Example 3.3, the Brillouin threshold occurs at an optical power level of around 80 mW while the Raman threshold is approximately 17 times larger. It is therefore apparent that the losses introduced by nonlinear scattering may be avoided by use of a suitable optical signal level (i.e. working below the threshold optical powers). However, it must be noted that the Brillouin threshold has been reported [Ref. 17] as occurring at optical powers as low as 10 mW in single-mode fibers. Nevertheless, this is still a high power level for optical communications and may be easily avoided. SBS and SRS are not usually observed in multimode fibers because their relatively large core diameters make the threshold optical power levels extremely high. Moreover, it should be noted that the threshold optical powers for both these scattering mechanisms may be increased by suitable adjustment of the other parameters in Eqs (3.6) and (3.7). In this context, operation at the longest possible wavelength is advantageous although this may be offset by the reduced fiber attenuation (from Rayleigh scattering and material absorption) normally obtained.

3.6 Fiber bend loss

Optical fibers suffer radiation losses at bends or curves on their paths. This is due to the energy in the evanescent field at the bend exceeding the velocity of light in the cladding and hence the guidance mechanism is inhibited, which causes light energy to be radiated from the fiber. An illustration of this situation is shown in Figure 3.5. The part of the mode which is on the outside of the bend is required to travel faster than that on the inside so that a wavefront perpendicular to the direction of propagation is maintained. Hence, part of the mode in the cladding needs to travel faster than the velocity of light in that medium. As this is not possible, the energy associated with this part of the mode is lost through radiation. The loss can generally be represented by a radiation attenuation coefficient which has the form [Ref. 18]:

$$\alpha_r = c_1 \exp(-c_2 R)$$

where R is the radius of curvature of the fiber bend and c_1, c_2 are constants which are independent of R. Furthermore, large bending losses tend to occur in multimode fibers at a critical radius of curvature R_c which may be estimated from [Ref. 19]:

$$R_c \approx \frac{3n^1\lambda}{4\pi(n^1 - n^2)^{3-2}} \tag{3.8}$$

It may be observed from the expression given in Eq. (3.8) that potential macrobending losses may be reduced by:

(a) designing fibers with large relative refractive index differences;

(b) operating at the shortest wavelength possible.

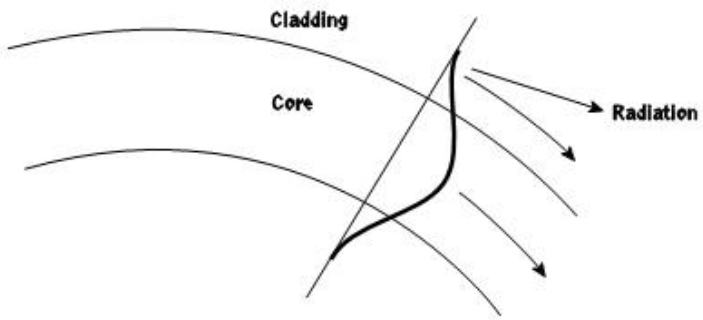

Figure 3.5 An illustration of the radiation loss at a fiber bend. The part of the mode in the cladding outside the dashed arrowed line may be required to travel faster than the velocity of light in order to maintain a plane wavefront. Since it cannot do this, the energy contained in this part of the mode is radiated away

The above criteria for the reduction of bend losses also apply to single-mode fibers. One theory [Ref. 20], based on the concept of a single quasi-guided mode, provides an expression from which the critical radius of curvature for a single-mode fiber R_{cs} can be estimated as:

$$R_{cs} \approx \frac{20\lambda}{(n_1 - n_2)^{3/2}}\left(2.748 - 0.996\left(\frac{\lambda}{\lambda_c}\right)^{-3}\right) \tag{3.9}$$

where λ_c is the cutoff wavelength for the single-mode fiber. Hence again, for a specific single-mode fiber (i.e. a fixed relative index difference and cutoff wavelength), the critical wavelength of the radiated light becomes progressively shorter as the bend radius is decreased. The effect of this factor and that of the relative refractive index difference on the critical bending radius is demonstrated in the following example.

Example 3.4

Two step index fibers exhibit the following parameters:

(a) a multimode fiber with a core refractive index of 1.500, a relative refractive index difference of 3% and an operating wavelength of 0.82 μm;

(b) an 8 μm core diameter single-mode fiber with a core refractive index the same as (a), a relative refractive index difference of 0.3% and an operating wavelength of 1.55 μm.

Estimate the critical radius of curvature at which large bending losses occur in both cases.

Solution: (a) The relative refractive index difference is given by Eq. (2.9) as:

$$\Delta = \frac{n^1 - n^2}{2n^1}$$

Hence:

$$n^2 = n^1 - 2\Delta n^1 = 2.250 - 0.06 \times 2.250 = 2.115$$

Using Eq. (3.8) for the multimode fiber critical radius of curvature:

$$R_c \approx \frac{3n^1\lambda}{4\pi(n^1 - n^2)^{1/2}} = \frac{3 \times 2.250 \times 0.82 \times 10^{-6}}{4\pi \times (0.135)^{1/2}} = 9\ \mu\text{m}$$

(b) Again, from Eq. (2.9):

$$n^2 = n^1 - 2\Delta n^1 = 2.250 - (0.006 \times 2.250)$$
$$= 2.237$$

The cutoff wavelength for the single-mode fiber is given by Eq. (2.98) as:

$$\lambda_c = \frac{2\pi a n_1 (2\Delta)^{1/2}}{2.405}$$

$$= \frac{2\pi \times 4 \times 10^{-6} \times 1.500\,(0.06)^{1/2}}{2.405}$$

$$= 1.214\ \mu\text{m}$$

Substituting into Eq. (3.9) for the critical radius of curvature for the single-mode fiber gives:

$$R_{cs} = \frac{20 \times 1.55 \times 10^{-6}}{(0.043)^{3/2}} \left[2.748 - \frac{0.996 \times 1.55 \times 10^{-6}}{1.214 \times 10^{-6}}\right]^{-3}$$
$$= 34\ \text{mm}$$

Example 3.4 shows that the critical radius of curvature for guided modes can be made extremely small (e.g. 9 μm), although this may be in conflict with the preferred design and operational characteristics. Nevertheless, for most practical purposes, the critical radius of curvature is relatively small (even when considering the case of a long-wavelength single-mode fiber, it was found to be around 34 mm) to avoid severe attenuation of the guided mode(s) at fiber bends. However, modes propagating close to cutoff, which are no longer fully guided within the fiber core, may radiate at substantially larger radii of curvature. Thus it is essential that sharp bends, with a radius of curvature approaching the critical radius, are avoided when optical fiber cables are installed. Finally, it is important that microscopic bends with radii of curvature approximating to the fiber radius are not produced in the fiber cabling process. These so-called microbends, which can cause significant losses from cabled fiber, are discussed further in Section 4.7.1.

3.7 Mid-infrared and far-infrared transmission

In the near-infrared region of the optical spectrum, fundamental silica fiber attenuation is dominated by Rayleigh scattering and multiphonon absorption from the infrared absorption edge (see Figure 3.2). Therefore, the total loss decreases as the operational transmission wavelength increases until a crossover point is reached around a wavelength of 1.55 μm where the total fiber loss again increases because at longer wavelengths the loss is dominated by the phonon absorption edge. Since the near fundamental attenuation limits for near-infrared silicate class fibers have been achieved, more recently researchers have turned their attention to the mid-infrared (2 to 5 μm) and the far-infrared (8 to 12 μm) optical wavelengths.

In order to obtain lower loss fibers it is necessary to produce glasses exhibiting longer infrared cutoff wavelengths. Potentially, much lower losses can be achieved if the transmission window of the material can be extended further into the infrared by utilizing constituent atoms of higher atomic mass and if it can be drawn into fiber exhibiting suitable strength and chemical durability. The reason for this possible loss reduction is due to Rayleigh scattering which displays a λ^{-4} dependence and hence becomes much reduced as the wavelength is increased. For example, the scattering loss is reduced by a factor of 16 when the optical wavelength is doubled. Thus it may be possible to obtain losses of the order of 0.01 dB km^{-1} at a wavelength of 2.55 μm, with even lower losses at wavelengths of between 3 and 5 μm [Ref. 21].

Candidate glass-forming systems for mid-infrared transmission are fluoride, fluoride-chloride, chalcogenide and oxide. In particular, oxide glasses such as Al_2O_3 (i.e. sapphire) offer a near equivalent transmittance range to many of the fluoride glasses and have benefits of high melting points, chemical inertness, and the ability to be readily melted and grown in air. Chalcogenide glasses, which generally comprise one or more elements Ge, Si, As and Sb, are capable of optical transmission in both the mid-infrared and far-infrared regions. A typical chalcogenide fiber glass is therefore arsenide trisulfide (As_2S_3). However, research activities into far-infrared transmission using chalcogenide glasses, halide glasses, polycrystalline halide fibers (e.g. silver and thallium) and hollow glass waveguides are primarily concerned with radiometry, infrared imaging, optical wireless, optical sensing and optical power transmission rather than telecommunications [Refs 22, 23].

Research activities into ultra-low-loss fibers for long-haul repeaterless communications in the 1980s and early 1990s centered on the fluorozirconates, with zirconium fluoride (ZrF_4) as the major constituent, and fluorides of barium, lanthanum, aluminum, gadolinium, sodium, lithium and occasionally lead added as modifiers and stabilizers [Ref. 24]. Such alkali additives improve the glass stability and working characteristics. Moreover, the two most popular heavy metal fluoride glasses for fabrication into fiber are fluorozirconate and fluoroaluminate glasses [Ref. 4]. Extensive work has been undertaken on a common fluorozirconate system comprising ZrF_4-BaF_2-LaF_3-AlF_3-NaF which forms ZBLAN, while an important fluoroaluminate comprises AlF_3-ZrF_4-BaF_2-CaF_3-YF_3. Although ZBLAN can theoretically provide for the lowest transmission losses over the mid-infrared wavelength region, it has a significantly lower glass transition (melting) temperature than the fluoroaluminate glass and is therefore less durable when subject to both thermal and mechanical perturbations.

The fabrication of low-loss, long-length fluoride fibers presents a basic problem with reducing the extrinsic losses which remains to be resolved [Refs 4, 25]. In practice, however, the most critical and difficult problems are associated with the minimization of the scattering losses resulting from extrinsic factors such as defects, waveguide imperfections and radiation caused by mechanical deformation. The estimated losses of around 0.01 dB km^{-1} at a wavelength of 2.55 μm for ZrF_4-based fibers are derived from an extrapolation of the intrinsic losses due to ultraviolet and infrared absorptions together with Rayleigh scattering [Ref. 21]. Moreover, refinements of scattering loss have increased this loss value slightly to 0.024 dB km^{-1} which is still around eight times lower than that of a silica fiber [Ref. 26]. Nevertheless, practical fiber losses remain much higher, as may be observed from the attenuation spectra for the common mid- and far-infrared fibers shown in Figure 3.6 in which the fluoride fiber (ZBLAN) is exhibiting a loss of several decibels per kilometer [Ref. 4].

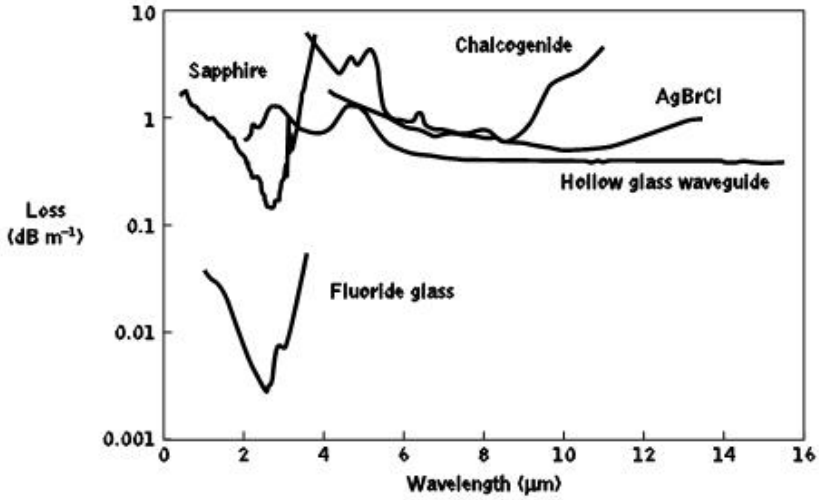

Figure 3.6 Attenuation spectra for some common mid- and far-infrared fibers [Ref. 4]

The loss spectrum for a single-crystal sapphire fiber which also transmits in the mid-infrared is also shown in Figure 3.6. Although they have robust physical properties, including a Young's modulus six times greater as well as a thermal expansion some ten times higher than that of silica, these fibers lend themselves to optical power delivery applications [Ref. 27], not specifically optical communications. Chalcogenide glasses which have their lowest losses over both the mid- and far-infrared ranges are very stable, durable and insensitive to moisture. Arsenic trisulfide fiber, being one of the simplest, has a spectral range from 0.7 to around 6 μm. Hence it has a cut off at long wavelength significantly before the chalcogenide fibers containing heavier elements such as Te, Ge and Se, an attenuation spectrum for the latter being incorporated in Figure 3.6. In general, chalcogenide glass fibers have proved to be useful in areas such as optical sensing, infrared imaging and for the production of fiber infrared lasers and amplifiers.

The loss spectrum for the polycrystalline fiber AgBrCl is also displayed in Figure 3.6. Although these fibers are transmissive over the entire far-infrared wavelength region and they were initially considered to hold significant potential as ultra-low-loss fibers because their intrinsic losses were estimated to be around 10^{-3} dB m^{-1} [Ref. 4], they are mechanically weak in comparison with silica fibers. In addition, the estimated low losses are far from being achieved, with experimental loss values being not even close to the predicted minimum as can be observed in Figure 3.6. Furthermore, polycrystalline fibers plastically deform resulting in increased transmission loss well before they fracture.

Finally, a hollow glass waveguide spectral characteristic is also shown in Figure 3.6. This hollow glass tube with a 530 μm bore was designed for optimum response at a transmission wavelength of 10 μm [Ref. 4]. Such hollow glass waveguides have been successfully employed for infrared laser power delivery at both 2.94 μm (Er:YAG laser) and 10.6 μm (CO_2 laser) [Ref. 28]. In summary, the remaining limitations of high loss (in comparison with theory) and low strength have inhibited the prospect of long-distance

mid- or far-infrared transmission for communications for even the most promising fluoride fibers, while a range of alternative nontelecommunications applications for the various fiber and waveguide types have been developed.

3.8 Dispersion

Dispersion of the transmitted optical signal causes distortion for both digital and analog transmission along optical fibers. When considering the major implementation of optical fiber transmission which involves some form of digital modulation, then dispersion mechanisms within the fiber cause broadening of the transmitted light pulses as they travel along the channel. The phenomenon is illustrated in Figure 3.7, where it may be observed that each pulse broadens and overlaps with its neighbors, eventually becoming indistinguishable at the receiver input. The effect is known as intersymbol interference (ISI). Thus an increasing number of errors may be encountered on the digital optical channel as the ISI becomes more pronounced. The error rate is also a function of the signal attenuation on the link and the subsequent signal-to-noise ratio (SNR) at the receiver. This factor is not pursued further here but is considered in detail in Section 12.6.3. However, signal dispersion alone limits the maximum possible bandwidth attainable with a particular optical fiber to the point where individual symbols can no longer be distinguished.

For no overlapping of light pulses down on an optical fiber link the digital bit rate B_T must be less than the reciprocal of the broadened (through dispersion) pulse duration (2τ). Hence:

$$B_T \leq \frac{1}{2\tau} \tag{3.10}$$

This assumes that the pulse broadening due to dispersion on the channel is τ which dictates the input pulse duration which is also τ. Hence Eq. (3.10) gives a conservative estimate of the maximum bit rate that may be obtained on an optical fiber link as $1/2\tau$.

Another more accurate estimate of the maximum bit rate for an optical channel with dispersion may be obtained by considering the light pulses at the output to have a Gaussian shape with an rms width of σ. Unlike the relationship given in Eq. (3.10), this analysis allows for the existence of a certain amount of signal overlap on the channel, while avoiding any SNR penalty which occurs when ISI becomes pronounced. The maximum bit rate is given approximately by (see Appendix B):

$$B_T(\max) \approx \frac{0.2}{\sigma} \text{ bit s}^{-1} \tag{3.11}$$

It must be noted that certain sources [Refs 29, 30] give the constant term in the numerator of Eq. (3.11) as 0.25. However, we take the slightly more conservative estimate given, following Olshansky [Ref. 11] and Gambling *et al.* [Ref. 31]. Equation (3.11) gives a reasonably good approximation for other pulse shapes which may occur on the channel resulting from the various dispersive mechanisms within the fiber. Also, σ may be

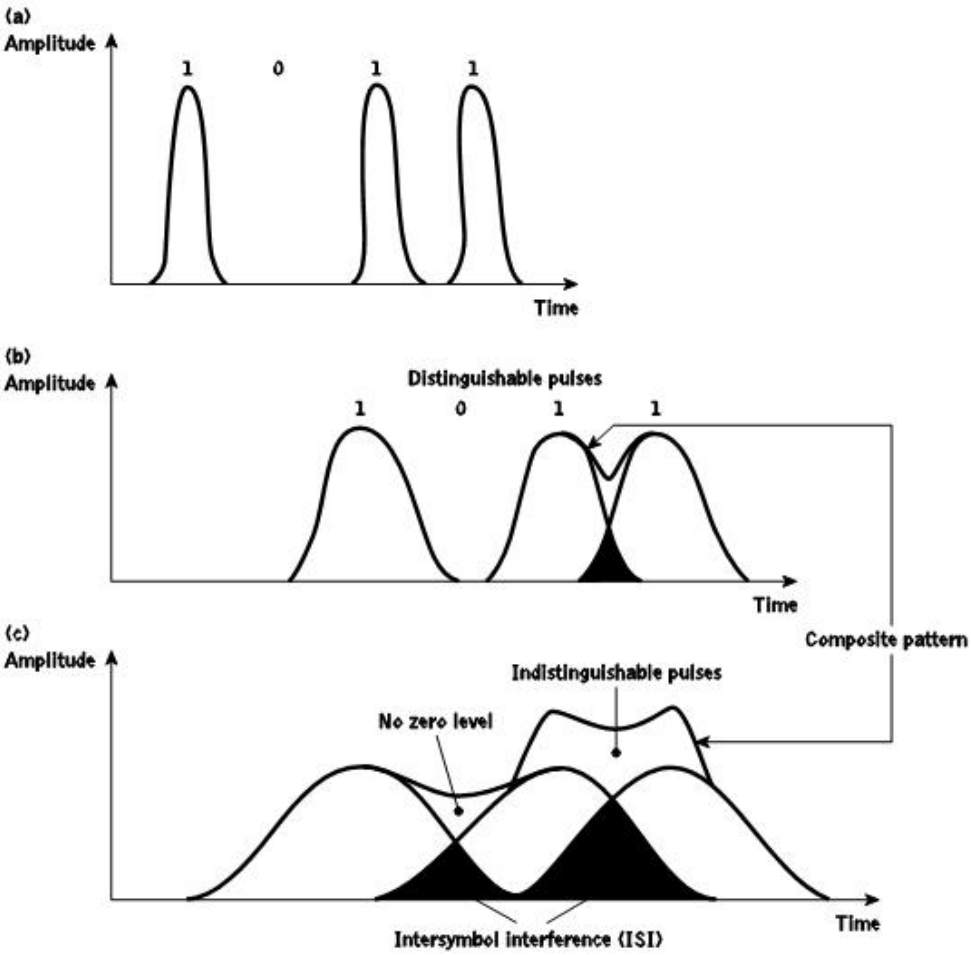

Figure 3.7 An illustration using the digital bit pattern 1011 of the broadening of light pulses as they are transmitted along a fiber: (a) fiber input; (b) fiber output at a distance L_1; (c) fiber output at a distance $L_2 > L_1$

assumed to represent the rms impulse response for the channel, as discussed further in Section 3.10.1.

The conversion of bit rate to bandwidth in hertz depends on the digital coding format used. For metallic conductors when a nonreturn-to-zero code is employed, the binary 1 level is held for the whole bit period τ. In this case there are two bit periods in one wavelength (i.e. 2 bits per second per hertz), as illustrated in Figure 3.8(a). Hence the maximum bandwidth B is one-half the maximum data rate or:

$$B_T(\max) = 2B \tag{3.12}$$

However, when a return-to-zero code is considered, as shown in Figure 3.8(b), the binary 1 level is held for only part (usually half) of the bit period. For this signaling scheme the

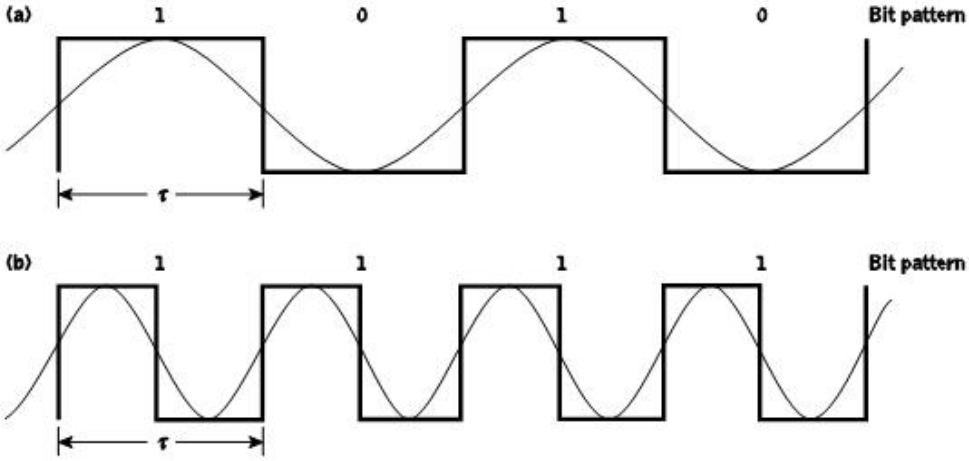

Figure 3.8 Schematic illustration of the relationships of the bit rate to wavelength for digital codes: (a) nonreturn-to-zero (NRZ); (b) return-to-zero (RZ)

data rate is equal to the bandwidth in hertz (i.e. 1 bit per second per hertz) and thus $B_T = B$. The bandwidth B for metallic conductors is also usually defined by the electrical 3 dB points (i.e. the frequencies at which the electric power has dropped to one-half of its constant maximum value). However, when the 3 dB optical bandwidth of a fiber is considered it is significantly larger than the corresponding 3 dB electrical bandwidth for the reasons discussed in Section 7.4.3. Hence, when the limitations in the bandwidth of a fiber due to dispersion are stated (i.e. optical bandwidth B_{opt}), it is usually with regard to a return to zero code where the bandwidth in hertz is considered equal to the digital bit rate. Within the context of dispersion the bandwidths expressed in this chapter will follow this general criterion unless otherwise stated. However, as is made clear in Section 7.4.3, when electro-optic devices and optical fiber systems are considered it is more usual to state the electrical 3 dB bandwidth, this being the more useful measurement when interfacing an optical fiber link to electrical terminal equipment. Unfortunately, the terms of bandwidth measurement are not always made clear and the reader must be warned that this omission may lead to some confusion when specifying components and materials for optical fiber communication systems.

Figure 3.9 shows the three common optical fiber structures, namely multimode step index, multimode graded index and single-mode step index, while diagrammatically illustrating the respective pulse broadening associated with each fiber type. It may be observed that the multimode step index fiber exhibits the greatest dispersion of a transmitted light pulse and the multimode graded index fiber gives a considerably improved performance. Finally, the single-mode fiber gives the minimum pulse broadening and thus is capable of the greatest transmission bandwidths which are currently in the gigahertz range, whereas transmission via multimode step index fiber is usually limited to bandwidths of a few tens of megahertz. However, the amount of pulse broadening is dependent upon the distance the pulse travels within the fiber, and hence for a given optical fiber link the restriction on usable bandwidth is dictated by the distance between regenerative repeaters (i.e. the

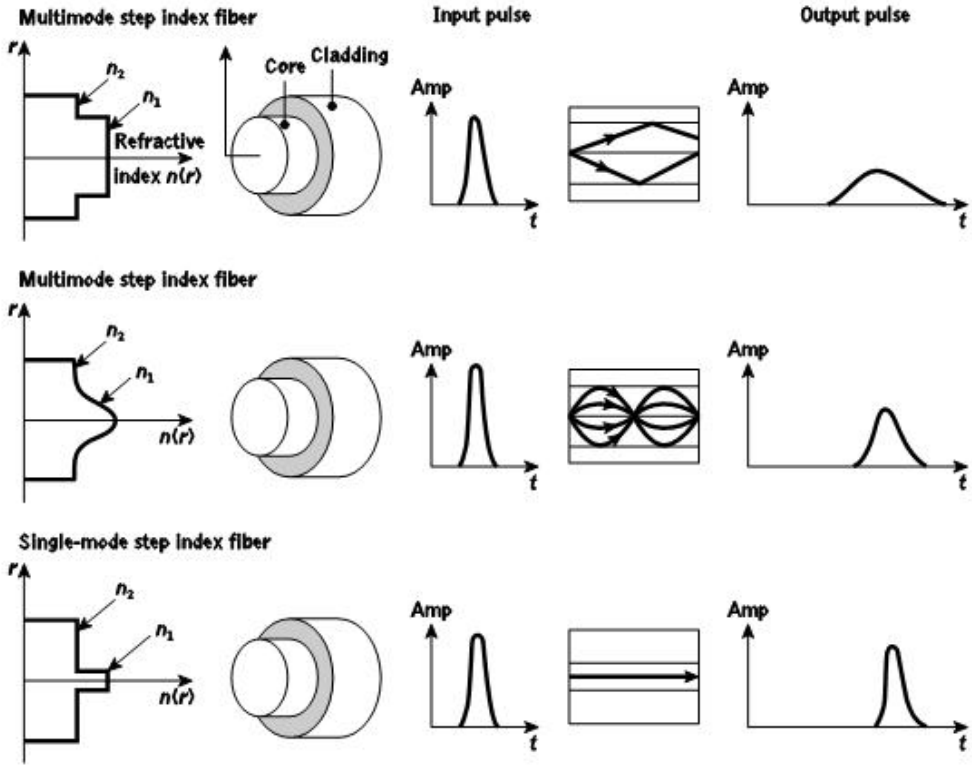

Figure 3.9 Schematic diagram showing a multimode step index fiber, multimode graded index fiber and single-mode step index fiber, and illustrating the pulse broadening due to intermodal dispersion in each fiber type

distance the light pulse travels before it is reconstituted). Thus the measurement of the dispersive properties of a particular fiber is usually stated as the pulse broadening in time over a unit length of the fiber (i.e. ns km^{-1}).

Hence, the number of optical signal pulses which may be transmitted in a given period, and therefore the information-carrying capacity of the fiber, is restricted by the amount of pulse dispersion per unit length. In the absence of mode coupling or filtering, the pulse broadening increases linearly with fiber length and thus the bandwidth is inversely proportional to distance. This leads to the adoption of a more useful parameter for the information-carrying capacity of an optical fiber which is known as the bandwidth-length product (i.e. $B_{opt} \times L$). The typical best bandwidth-length products for the three fibers shown in Figure 3.9 are 20 MHz km, 1 GHz km and 100 GHz km for multimode step index, multimode graded index and single-mode step index fibers respectively.

In order to appreciate the reasons for the different amounts of pulse broadening within the various types of optical fiber, it is necessary to consider the dispersive mechanisms involved. These include material dispersion, waveguide dispersion, intermodal dispersion and profile dispersion which are considered in the following sections.

Example 3.5

A multimode graded index fiber exhibits total pulse broadening of 0.1 μs over a distance of 15 km. Estimate:

(a) the maximum possible bandwidth on the link assuming no intersymbol interference;

(b) the pulse dispersion per unit length;

(c) the bandwidth-length product for the fiber.

Solution: (a) The maximum possible optical bandwidth which is equivalent to the maximum possible bit rate (for return to zero pulses) assuming no ISI may be obtained from Eq. (3.10), where:

$$B_{\text{opt}} = B_{\text{T}} = \frac{1}{2\tau} = \frac{1}{0.2 \times 10_{-6}} = 5 \text{ MHz}$$

(b) The dispersion per unit length may be acquired simply by dividing the total dispersion by the total length of the fiber:

$$\text{Dispersion} = \frac{0.1 \times 10^{-6}}{15} = 6.67 \text{ ns km}^{-1}$$

(c) The bandwidth-length product may be obtained in two ways. Firstly by simply multiplying the maximum bandwidth for the fiber link by its length. Hence:

$$B_{\text{opt}} L = 5 \text{ MHz} \times 15 \text{ km} = 75 \text{ MHz km}$$

Alternatively, it may be obtained from the dispersion per unit length using Eq. (3.10) where:

$$B_{\text{opt}} L = \frac{1}{2 \times 6.67 \times 10^{-6}} = 75 \text{ MHz km}$$

3.9 Chromatic dispersion

Chromatic or intramodal dispersion may occur in all types of optical fiber and results from the finite spectral linewidth of the optical source. Since optical sources do not emit just a single frequency but a band of frequencies (in the case of the injection laser corresponding to only a fraction of a percent of the center frequency, whereas for the LED it is likely to be a significant percentage), then there may be propagation delay differences between the

different spectral components of the transmitted signal. This causes broadening of each transmitted mode and hence intramodal dispersion. The delay differences may be caused by the dispersive properties of the waveguide material (material dispersion) and also guidance effects within the fiber structure (waveguide dispersion).

3.9.1 Material dispersion

Pulse broadening due to material dispersion results from the different group velocities of the various spectral components launched into the fiber from the optical source. It occurs when the phase velocity of a plane wave propagating in the dielectric medium varies non-linearly with wavelength, and a material is said to exhibit material dispersion when the second differential of the refractive index with respect to wavelength is not zero (i.e. $d^2n/d\lambda^2 \neq 0$). The pulse spread due to material dispersion may be obtained by considering the group delay τ_g in the optical fiber which is the reciprocal of the group velocity υ_g defined by Eqs (2.37) and (2.40). Hence the group delay is given by:

$$\tau_g = \frac{d\beta}{d\omega} = \frac{1}{c}\left(n_1 - \lambda \frac{dn_1}{d\lambda}\right) \tag{3.13}$$

where n_1 is the refractive index of the core material. The pulse delay τ_m due to material dispersion in a fiber of length L is therefore:

$$\tau_m = \frac{L}{c}\left(n_1 - \lambda \frac{dn_1}{d\lambda}\right) \tag{3.14}$$

For a source with rms spectral width σ_λ and a mean wavelength λ, the rms pulse broadening due to material dispersion σ_m may be obtained from the expansion of Eq. (3.14) in a Taylor series about λ where:

$$\sigma_m = \sigma_\lambda \frac{d\tau_m}{d\lambda} + \sigma_\lambda \frac{2d^2\tau_m}{d\lambda^2} + \ldots \tag{3.15}$$

As the first term in Eq. (3.15) usually dominates, especially for sources operating over the 0.8 to 0.9 μm wavelength range, then:

$$\sigma_m \approx \sigma_\lambda \frac{d\tau_m}{d\lambda} \tag{3.16}$$

Hence the pulse spread may be evaluated by considering the dependence of τ_m on λ, where from Eq. (3.14):

$$\frac{d\tau_m}{d\lambda} = \frac{L\lambda}{c}\left(\frac{dn_1}{d\lambda} - \frac{d^2n_1}{d\lambda^2}\right) - \frac{dn_1}{d\lambda}$$

$$= \frac{-L\lambda}{c}\frac{d^2n_1}{d\lambda^2} \tag{3.17}$$

Therefore, substituting the expression obtained in Eq. (3.17) into Eq. (3.16), the rms pulse broadening due to material dispersion is given by:

$$\sigma_m \approx \frac{L}{c}\,\sigma_\lambda \lambda^2 \frac{d^2 n_1}{d\lambda^2} \tag{3.18}$$

The material dispersion for optical fibers is sometimes quoted as a value for $|\lambda^2(d^2n_1/d\lambda^2)|$ or simply $|d^2n_1/d\lambda^2|$.

However, it may be given in terms of a material dispersion parameter M which is defined as:

$$M = \frac{1}{L}\frac{d\tau_m}{d\lambda} = \frac{\lambda}{c}\frac{d^2 n_1}{d\lambda^2} \tag{3.19}$$

and which is often expressed in units of ps nm^{-1} km^{-1}.

Example 3.6

A glass fiber exhibits material dispersion given by $|\lambda^2(d^2n_1/d\lambda^2)|$ of 0.025. Determine the material dispersion parameter at a wavelength of 0.85 μm, and estimate the rms pulse broadening per kilometer for a good LED source with an rms spectral width of 20 nm at this wavelength.

Solution: The material dispersion parameter may be obtained from Eq. (3.19):

$$M = \frac{\lambda}{c}\frac{d^2 n_1}{d\lambda^2} = \frac{1}{c\lambda}\lambda^2 \frac{d^2 n_1}{d\lambda^2}$$

$$= \frac{0.025}{2.998 \times 10^5 \times 850} \text{ s nm}^{-1} \text{ km}^{-1}$$

$$= 98.1 \text{ ps nm}^{-1} \text{ km}^{-1}$$

The rms pulse broadening is given by Eq. (3.18) as:

$$\sigma_m \approx \frac{L}{c}\,\sigma_\lambda \lambda^2 \frac{d^2 n_1}{d\lambda^2}$$

Therefore in terms of the material dispersion parameter M defined by Eq. (3.19):

$$\sigma_m \approx \sigma_\lambda LM$$

Hence, the rms pulse broadening per kilometer due to material dispersion:

$$\sigma_m (1 \text{ km}) = 20 \times 1 \times 98.1 \times 10^{-12} = 1.96 \text{ ns km}^{-1}$$

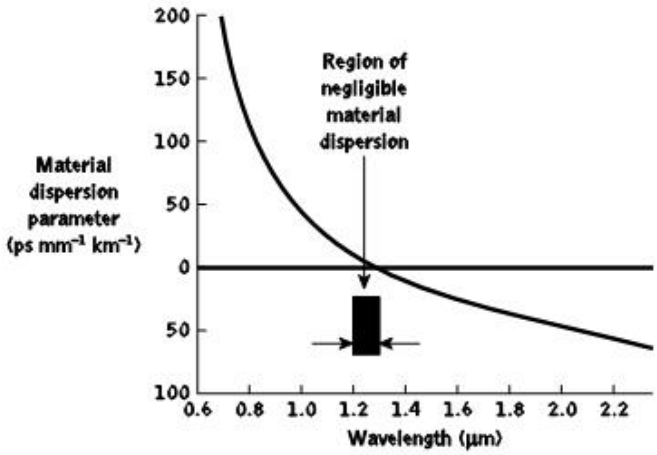

Figure 3.10 The material dispersion parameter for silica as a function of wavelength. Reproduced with permission from D. N. Payne and W. A. Gambling, *Electron. Lett.*, 11, p. 176, 1975

Figure 3.10 shows the variation of the material dispersion parameter M with wavelength for pure silica [Ref. 32]. It may be observed that the material dispersion tends to zero in the longer wavelength region around 1.3 μm (for pure silica). This provides an additional incentive (other than low attenuation) for operation at longer wavelengths where the material dispersion may be minimized. Also, the use of an injection laser with a narrow spectral width rather than an LED as the optical source leads to a substantial reduction in the pulse broadening due to material dispersion, even in the shorter wavelength region.

Example 3.7

Estimate the rms pulse broadening per kilometer for the fiber in Example 3.6 when the optical source used is an injection laser with a relative spectral width σ_λ/λ of 0.0012 at a wavelength of 0.85 μm.

Solution: The rms spectral width may be obtained from the relative spectral width by:

$$\sigma_\lambda = 0.0012\lambda = 0.0012 \times 0.85 \times 10_{-6}$$
$$= 1.02 \text{ nm}$$

The rms pulse broadening in terms of the material dispersion parameter following Example 3.6 is given by:

$$\sigma_m \quad \sigma_\lambda LM$$

Therefore, the rms pulse broadening per kilometer due to material dispersion is:

$$\sigma_m 1.02 \times 1 \times 98.1 \times 10^{-12} = 0.10 \text{ ns km}^{-1}$$

Hence, in this example the rms pulse broadening is reduced by a factor of around 20 (i.e. equivalent to the reduced rms spectral width of the injection laser source) compared with that obtained with the LED source of Example 3.6.

3.9.2 Waveguide dispersion

The waveguiding of the fiber may also create chromatic dispersion. This results from the variation in group velocity with wavelength for a particular mode. Considering the ray theory approach, it is equivalent to the angle between the ray and the fiber axis varying with wavelength which subsequently leads to a variation in the transmission times for the rays, and hence dispersion. For a single mode whose propagation constant is β, the fiber exhibits waveguide dispersion when $d^2\beta/d\lambda^2 \neq 0$. Multimode fibers, where the majority of modes propagate far from cutoff, are almost free of waveguide dispersion and it is generally negligible compared with material dispersion ($\approx$0.1 to 0.2 ns km^{-1}) [Ref. 32]. However, with single-mode fibers where the effects of the different dispersion mechanisms are not easy to separate, waveguide dispersion may be significant (see Section 3.11.2).

3.10 Intermodal dispersion

Pulse broadening due to intermodal dispersion (sometimes referred to simply as modal or mode dispersion) results from the propagation delay differences between modes within a multimode fiber. As the different modes which constitute a pulse in a multimode fiber travel along the channel at different group velocities, the pulse width at the output is dependent upon the transmission times of the slowest and fastest modes. This dispersion mechanism creates the fundamental difference in the overall dispersion for the three types of fiber shown in Figure 3.9. Thus multimode step index fibers exhibit a large amount of intermodal dispersion which gives the greatest pulse broadening. However, intermodal dispersion in multimode fibers may be reduced by adoption of an optimum refractive index profile which is provided by the near-parabolic profile of most graded index fibers. Hence, the overall pulse broadening in multimode graded index fibers is far less than that obtained in multimode step index fibers (typically by a factor of 100). Thus graded index fibers used with a multimode source give a tremendous bandwidth advantage over multimode step index fibers.

Under purely single-mode operation there is no intermodal dispersion and therefore pulse broadening is solely due to the intramodal dispersion mechanisms. In theory, this is the case with single-mode step index fibers where only a single mode is allowed to propagate. Hence they exhibit the least pulse broadening and have the greatest possible bandwidths, but in general are only usefully operated with single-mode sources.

In order to obtain a simple comparison for intermodal pulse broadening between multimode step index and multimode graded index fibers, it is useful to consider the geometric optics picture for the two types of fiber.

3.10.1 Multimode step index fiber

Using the ray theory model, the fastest and slowest modes propagating in the step index fiber may be represented by the axial ray and the extreme meridional ray (which is incident at the core-cladding interface at the critical angle φ_c) respectively. The paths taken by these two rays in a perfectly structured step index fiber are shown in Figure 3.11. The delay difference between these two rays when traveling in the fiber core allows estimation of the pulse broadening resulting from intermodal dispersion within the fiber. As both rays are traveling at the same velocity within the constant refractive index fiber core, then the delay difference is directly related to their respective path lengths within the fiber. Hence the time taken for the axial ray to travel along a fiber of length L gives the minimum delay time T_{Min} and:

$$T_{\text{Min}} = \frac{\text{distance}}{\text{velocity}} = \frac{L}{(c/n_1)} = \frac{Ln_1}{c} \tag{3.20}$$

where n_1 is the refractive index of the core and c is the velocity of light in a vacuum.

The extreme meridional ray exhibits the maximum delay time T_{Max} where:

$$T_{\text{Max}} = \frac{L/\cos\theta}{c/n_1} = \frac{Ln_1}{c\cos\theta} \tag{3.21}$$

Using Snell's law of refraction at the core-cladding interface following Eq. (2.2):

$$\sin\varphi_c = \frac{n_2}{n_1} = \cos\theta \tag{3.22}$$

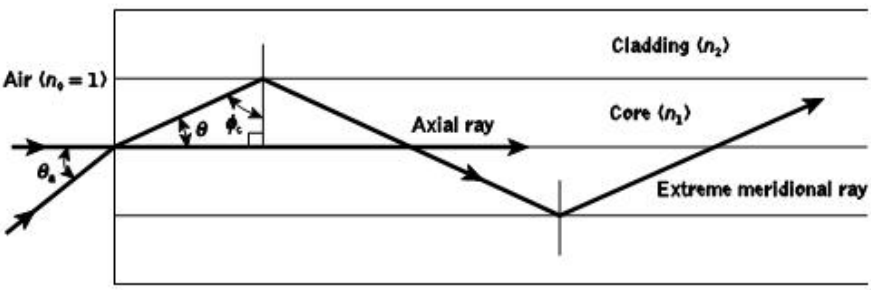

Figure 3.11 The paths taken by the axial and an extreme meridional ray in a perfect multimode step index fiber

where n_2 is the refractive index of the cladding. Furthermore, substituting into Eq. (3.21) for $\cos\theta$ gives:

$$T_{\text{Max}} = \frac{Ln^1}{cn_2} \tag{3.23}$$

The delay difference δT_s between the extreme meridional ray and the axial ray may be obtained by subtracting Eq. (3.20) from Eq. (3.23). Hence:

$$\delta T_s = T_{\text{Max}} - T_{\text{Min}} = \frac{Ln^1}{cn_2} - \frac{Ln_1}{c}$$

$$= \frac{Ln^1}{cn_2}\left(\frac{n_1 - n_2}{n_1}\right) \tag{3.24}$$

$$\frac{Ln^1\Delta}{cn_2} \quad \text{when } \Delta \quad 1 \tag{3.25}$$

where Δ is the relative refractive index difference. However, when Δ 1, then from the definition given by Eq. (2.9), the relative refractive index difference may also be given approximately by:

$$\Delta \quad \frac{n_1 - n_2}{n_2} \tag{3.26}$$

Hence rearranging Eq. (3.24):

$$\delta T_s = \frac{Ln_1}{c}\left(\frac{n_1 - n_2}{n_2}\right) \quad \frac{Ln_1\Delta}{c} \tag{3.27}$$

Also substituting for Δ from Eq. (2.10) gives:

$$\delta T_s \quad \frac{L(NA)^2}{2n_1c} \tag{3.28}$$

where NA is the numerical aperture for the fiber. The approximate expressions for the delay difference given in Eqs (3.27) and (3.28) are usually employed to estimate the maximum pulse broadening in time due to intermodal dispersion in multimode step index fibers. It must be noted that this simple analysis only considers pulse broadening due to meridional rays and totally ignores skew rays with acceptance angles $\theta_{as} > \theta_a$ (see Section 2.2.4).

Again considering the perfect step index fiber, another useful quantity with regard to intermodal dispersion on an optical fiber link is the rms pulse broadening resulting from this dispersion mechanism along the fiber. When the optical input to the fiber is a pulse $p_i(t)$ of unit area, as illustrated in Figure 3.12, then [Ref. 33]:

$$\int_{-\infty}^{\infty} p_i(t)\,dt = 1 \tag{3.29}$$

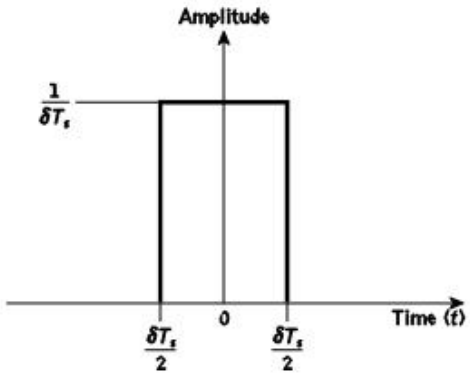

Figure 3.12 An illustration of the light input to the multimode step index fiber consisting of an ideal pulse or rectangular function with unit area

It may be noted that $p_i(t)$ has a constant amplitude of $1/\delta T_s$ over the range:

$$\frac{-\delta T_s}{2} \leq p(t) \leq \frac{\delta T_s}{2}$$

The rms pulse broadening at the fiber output due to intermodal dispersion for the multimode step index fiber σ_s (i.e. the standard deviation) may be given in terms of the variance σ^s as (see Appendix C):

$$\sigma^s = M_2 - M^1 \tag{3.30}$$

where M_1 is the first temporal moment which is equivalent to the mean value of the pulse and M_2, the second temporal moment, is equivalent to the mean square value of the pulse. Hence:

$$M_1 = \int_{-\infty}^{\infty} t p_i(t)\, dt \tag{3.31}$$

and:

$$M_2 = \int_{-\infty}^{\infty} t^2 p_i(t)\, dt \tag{3.32}$$

The mean value M_1 for the unit input pulse of Figure 3.12 is zero, and assuming this is maintained for the output pulse, then from Eqs (3.30) and (3.32):

$$\sigma^s = M_2 = \int_{-\infty}^{\infty} t^2 p_i(t)\, dt \tag{3.33}$$

Integrating over the limits of the input pulse (Figure 3.12) and substituting for $p_i(t)$ in Eq. (3.33) over this range gives:

$$\sigma_s^2 = \int_{-\delta T_s/2}^{\delta T_s/2} \frac{1}{\delta T_s} t^2 \, dt$$

$$= \frac{1}{\delta T_s} \left[\frac{t^3}{3} \right]_{-\delta T_s/2}^{\delta T_s/2} = \frac{1}{3} \left(\frac{\delta T_s}{2} \right)^2 \tag{3.34}$$

Hence substituting from Eq. (3.27) for δT_s gives:

$$\sigma_s \approx \frac{Ln_1\Delta}{2\sqrt{3}c} \approx \frac{L(NA)^2}{4\sqrt{3}n_1 c} \tag{3.35}$$

Equation (3.35) allows estimation of the rms impulse response of a multimode step index fiber if it is assumed that intermodal dispersion dominates and there is a uniform distribution of light rays over the range $0 \leq \theta \leq \theta_a$. The pulse broadening is directly proportional to the relative refractive index difference Δ and the length of the fiber L. The latter emphasizes the bandwidth-length trade-off that exists, especially with multimode step index fibers, and which inhibits their use for wideband long-haul (between repeaters) systems. Furthermore, the pulse broadening is reduced by reduction of the relative refractive index difference Δ for the fiber. This suggests that weakly guiding fibers (see Section 2.4.1) with small Δ are best for low-dispersion transmission. However, as may be seen from Eq. (3.35) this is also subject to a trade-off as a reduction in Δ reduces the acceptance angle θ_a and the *NA*, thus worsening the launch conditions.

Example 3.8

A 6 km optical link consists of multimode step index fiber with a core refractive index of 1.5 and a relative refractive index difference of 1%. Estimate:

(a) the delay difference between the slowest and fastest modes at the fiber output;

(b) the rms pulse broadening due to intermodal dispersion on the link;

(c) the maximum bit rate that may be obtained without substantial errors on the link assuming only intermodal dispersion;

(d) the bandwidth-length product corresponding to (c).

Solution: (a) The delay difference is given by Eq. (3.27) as:

$$\delta T_s \approx \frac{Ln_1\Delta}{c} = \frac{6 \times 10^3 \times 1.5 \times 0.01}{2.998 \times 10^8}$$

$$= 300 \text{ ns}$$

(b) The rms pulse broadening due to intermodal dispersion may be obtained from Eq. (3.35) where:

$$\sigma_s = \frac{Ln_1\Delta}{2\sqrt{3}c} = \frac{1}{2\sqrt{3}} \frac{6 \times 10^3 \times 1.5 \times 0.01}{2.998 \times 10^8}$$

$$= 86.7 \text{ ns}$$

(c) The maximum bit rate may be estimated in two ways. Firstly, to get an idea of the maximum bit rate when assuming no pulse overlap, Eq. (3.10) may be used where:

$$B_T(\max) = \frac{1}{2\tau} = \frac{1}{2\delta T_s} = \frac{1}{600 \times 10^{-9}}$$

$$= 1.7 \text{ Mbit s}^{-1}$$

Alternatively an improved estimate may be obtained using the calculated rms pulse broadening in Eq. (3.11) where:

$$B_T(\max) = \frac{0.2}{\sigma_s} = \frac{0.2}{86.7 \times 10^{-9}}$$

$$= 2.3 \text{ Mbit s}^{-1}$$

(d) Using the most accurate estimate of the maximum bit rate from (c), and assuming return to zero pulses, the bandwidth-length product is:

$$B_{opt} \times L = 2.3 \text{ MHz} \times 6 \text{ km} = 13.8 \text{ MHz km}$$

Intermodal dispersion may be reduced by propagation mechanisms within practical fibers. For instance, there is differential attenuation of the various modes in a step index fiber. This is due to the greater field penetration of the higher order modes into the cladding of the waveguide. These slower modes therefore exhibit larger losses at any core-cladding irregularities, which tends to concentrate the transmitted optical power into the faster lower order modes. Thus the differential attenuation of modes reduces intermodal pulse broadening on a multimode optical link.

Another mechanism which reduces intermodal pulse broadening in nonperfect (i.e. practical) multimode fibers is the mode coupling or mixing discussed in Section 2.4.2. The coupling between guided modes transfers optical power from the slower to the faster modes, and vice versa. Hence, with strong coupling the optical power tends to be transmitted at an average speed, which is the mean of the various propagating modes. This reduces the intermodal dispersion on the link and makes it advantageous to encourage mode coupling within multimode fibers.

The expression for delay difference given in Eq. (3.27) for a perfect step index fiber may be modified for the fiber with mode coupling among all guided modes to [Ref. 34]:

$$\delta T_{sc} \quad \frac{n_1 \Delta}{c} (L L_c)^{1/2} \tag{3.36}$$

where L_c is a characteristic length for the fiber which is inversely proportional to the coupling strength. Hence, the delay difference increases at a slower rate proportional to $(LL_c)^{1/2}$ instead of the direct proportionality to L given in Eq. (3.27). However, the most successful technique for reducing intermodal dispersion in multimode fibers is by grading the core refractive index to follow a near-parabolic profile. This has the effect of equalizing the transmission times of the various modes as discussed in the following section.

3.10.2 Multimode graded index fiber

Intermodal dispersion in multimode fibers is minimized with the use of graded index fibers. Hence, multimode graded index fibers show substantial bandwidth improvement over multimode step index fibers. The reason for the improved performance of graded index fibers may be observed by considering the ray diagram for a graded index fiber shown in Figure 3.13. The fiber shown has a parabolic index profile with a maximum at the core axis, as illustrated in Figure 3.13(a). Analytically, the index profile is given by Eq. (2.75) with $\alpha = 2$ as:

$$n(r) = \begin{cases} n_1[1 - 2\Delta(r/a)^2]^{1/2} & r < a \text{ (core)} \\ = n_1(1 - 2\Delta)^{1/2} & r \geq a \text{ (cladding)} \end{cases} \tag{3.37}$$

Figure 3.13(b) shows several meridional ray paths within the fiber core. It may be observed that apart from the axial ray, the meridional rays follow sinusoidal trajectories of different path lengths which result from the index grading, as was discussed in Section 2.4.4. However, following Eq. (2.40) the local group velocity is inversely proportional to

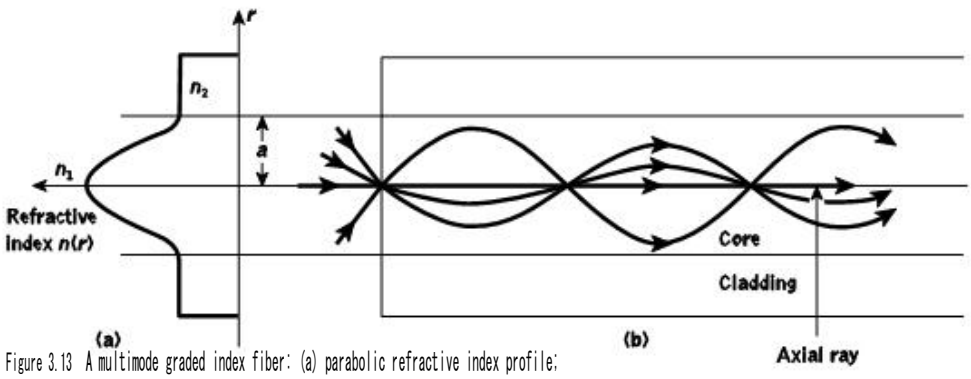

Figure 3.13 A multimode graded index fiber: (a) parabolic refractive index profile; (b) meridional ray paths within the fiber core

the local refractive index and therefore the longer sinusoidal paths are compensated for by higher speeds in the lower index medium away from the axis. Hence there is an equalization of the transmission times of the various trajectories towards the transmission time of the axial ray which travels exclusively in the high-index region at the core axis, and at the slowest speed. As these various ray paths may be considered to represent the different modes propagating in the fiber, then the graded profile reduces the disparity in the mode transit times.

The dramatic improvement in multimode fiber bandwidth achieved with a parabolic or near-parabolic refractive index profile is highlighted by consideration of the reduced delay difference between the fastest and slowest modes for this graded index fiber δT_g. Using a ray theory approach the delay difference is given by [Ref. 35]:

$$\delta T_g \quad \frac{Ln_1\Delta^2}{2c} \quad \frac{(NA)^4}{8n^1c} \tag{3.38}$$

As in the step index case, Eq. (2.10) is used for conversion between the two expressions shown.

However, a more rigorous analysis using electromagnetic mode theory gives an absolute temporal width at the fiber output of [Refs 36, 37]:

$$\delta T_g = \frac{Ln_1\Delta^2}{8c} \tag{3.39}$$

which corresponds to an increase in transmission time for the slowest mode of $\Delta^2/8$ over the fastest mode. The expression given in Eq. (3.39) does not restrict the bandwidth to pulses with time slots corresponding to δT_g as 70% of the optical power is concentrated in the first half of the interval. Hence the rms pulse broadening is a useful parameter for assessment of intermodal dispersion in multimode graded index fibers. It may be shown [Ref. 37] that the rms pulse broadening of a near-parabolic index profile graded index fiber σ_g is reduced compared with similar broadening for the corresponding step index fiber σ_s (i.e. with the same relative refractive index difference) following:

$$\sigma_g = \frac{\Delta}{} \sigma_s D \tag{3.40}$$

where D is a constant between 4 and 10 depending on the precise evaluation and the exact optimum profile chosen.

The best minimum theoretical intermodal rms pulse broadening for a graded index fiber with an optimum characteristic refractive index profile for the core α_{op} of [Refs 37, 38]:

$$\alpha_{op} = 2 - \frac{12\Delta}{5} \tag{3.41}$$

is given by combining Eqs (3.27) and (3.40) as [Refs 31, 38]:

$$\sigma_g = \frac{Ln_1\Delta^2}{20\sqrt{3}c} \tag{3.42}$$

Example 3.9

Compare the rms pulse broadening per kilometer due to intermodal dispersion for the multimode step index fiber of Example 3.8 with the corresponding rms pulse broadening for an optimum near-parabolic profile graded index fiber with the same core axis refractive index and relative refractive index difference.

Solution: In Example 3.8, σ_s over 6 km of fiber is 86.7 ns. Hence the rms pulse broadening per kilometer for the multimode step index fiber is:

$$\frac{\sigma_s(1\text{ km})}{L} = \frac{86.7}{6} = 14.4\text{ ns km}^{-1}$$

Using Eq. (3.42), the rms pulse broadening per kilometer for the corresponding graded index fiber is:

$$\sigma_g(1\text{ km}) = \frac{Ln_1\Delta^2}{20\sqrt{3}c} = \frac{10^3 \times 1.5 \times (0.01)^2}{20\sqrt{3} \times 2.998 \times 10^8}$$
$$= 14.4\text{ ps km}^{-1}$$

Hence, from Example 3.9, the theoretical improvement factor of the graded index fiber in relation to intermodal rms pulse broadening is 1000. However, this level of improvement is not usually achieved in practice due to difficulties in controlling the refractive index profile radially over long lengths of fiber. Any deviation in the refractive index profile from the optimum results in increased intermodal pulse broadening. This may be observed from the curve shown in Figure 3.14, which gives the variation in intermodal pulse broadening (δT_g) as a function of the characteristic refractive index profile α for typical graded

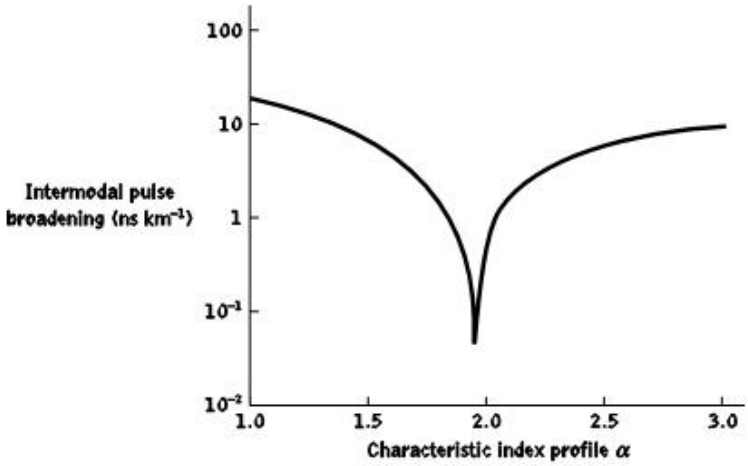

Figure 3.14 The intermodal pulse broadening δT_g for graded index fibers having $\Delta = 1\%$, against the characteristic refractive index profile α

index fibers (where $\Delta = 1\%$). The curve displays a sharp minimum at a characteristic refractive index profile slightly less than 2 ($\alpha = 1.98$). This corresponds to the optimum value of α in order to minimize intermodal dispersion. Furthermore, the extreme sensitivity of the intermodal pulse broadening to slight variations in α from this optimum value is evident. Thus at present improvement factors for practical graded index fibers over corresponding step index fibers with regard to intermodal dispersion are around 100 [Ref. 36].

Another important factor in the determination of the optimum refractive index profile for a graded index fiber is the dispersion incurred due to the difference in refractive index between the fiber core and cladding. It results from a variation in the refractive index profile with optical wavelength in the graded fiber and is often given by a profile dispersion parameter $d\Delta/d\lambda$. Thus the optimized profile at a given wavelength is not necessarily optimized at another wavelength. As all optical fiber sources (e.g. injection lasers and LEDs) have a finite spectral width, the profile shape must be altered to compensate for this dispersion mechanism. Moreover, the minimum overall dispersion for graded index fiber is also limited by the other intramodal dispersion mechanisms (i.e. material and waveguide dispersion). These give temporal pulse broadening of around 0.08 and 1 ns km^{-1} with injection lasers and LEDs respectively. Therefore, practical pulse broadening values for graded index fibers lie in the range 0.2 to 1 ns km^{-1}. This gives bandwidth-length products of between 0.5 and 2.5 GHz km when using lasers and optimum profile fiber.

3.10.3 Modal noise

The intermodal dispersion properties of multimode optical fibers (see Sections 3.10.1 and 3.10.2) create another phenomenon which affects the transmitted signals on the optical channel. It is exhibited within the speckle patterns observed in multimode fiber as fluctuations which have characteristic times longer than the resolution time of the detector, and is known as modal or speckle noise. The speckle patterns are formed by the interference of the modes from a coherent source when the coherence time of the source is greater than the intermodal dispersion time δT within the fiber. The coherence time for a source with uncorrelated source frequency width δf is simply $1/\delta f$. Hence, modal noise occurs when:

$$\delta f \quad \frac{1}{\delta T} \tag{3.43}$$

Disturbances along the fiber such as vibrations, discontinuities, connectors, splices and source/detector coupling may cause fluctuations in the speckle patterns and hence modal noise. It is generated when the correlation between two or more modes which gives the original interference is differentially delayed by these disturbances. The conditions which give rise to modal noise are therefore specified as:

(a) a coherent source with a narrow spectral width and long coherence length (propagation velocity multiplied by the coherence time);

(b) disturbances along the fiber which give differential mode delay or modal and spatial filtering;

(c) phase correlation between the modes.

Measurements [Ref. 39] of rms signal to modal noise ratio using good narrow-linewidth injection lasers show large signal-to-noise ratio penalties under the previously mentioned conditions. The measurements were carried out by misaligning connectors to create disturbances. They gave carrier to noise ratios reduced by around 10 dB when the attenuation at each connector was 20 dB due to substantial axial misalignment.

Modal noise may be avoided by removing one of the conditions (they must all be present) which give rise to this degradation. Hence modal-noise-free transmission may be obtained by the following:

1. The use of a broad spectrum source in order to eliminate the modal interference effects. This may be achieved by either (a) increasing the width of the single longitudinal mode and hence decreasing its coherence time or (b) by increasing the number of longitudinal modes and averaging out of the interference patterns [Ref. 40].
2. In conjunction with 1(b) it is found that fibers with large numerical apertures support the transmission of a large number of modes giving a greater number of speckles, and hence reduce the modal noise generating effect of individual speckles [Ref. 41].
3. The use of single-mode fiber which does not support the transmission of different modes and thus there is no intermodal interference.
4. The removal of disturbances along the fiber. This has been investigated with regard to connector design [Ref. 42] in order to reduce the shift in speckle pattern induced by mechanical vibration and fiber misalignment.

Hence, modal noise may be prevented on an optical fiber link through suitable choice of the system components. However, this may not always be possible and then certain levels of modal noise must be tolerated. This tends to be the case on high-quality analog optical fiber links where multimode injection lasers are frequently used. Analog transmission is also more susceptible to modal noise due to the higher optical power levels required at the receiver when quantum noise effects are considered (see Section 10.2.5). Therefore, it is important that modal noise is taken into account within the design considerations for these systems.

Modal noise, however, can be present in single-mode fiber links when propagation of the two fundamental modes with orthogonal polarization is allowed or, alternatively, when the second-order modes* are not sufficiently attenuated. The former modal noise type, which is known as polarization modal noise, is outlined in Section 3.13.1. For the latter type, it is apparent that at shorter wavelengths, a nominally single-mode fiber can also guide four second-order LP modes (see Section 2.4.1). Modal noise can therefore be introduced into single-mode fiber systems by time-varying interference between the LP_{01} and the LP_{11} modes when the fiber is operated at a wavelength which is smaller than the cutoff wavelength of the second-order modes. The effect has been observed in overmoded single-mode fibers [Ref. 43] and may be caused by a number of conditions. In particular

* In addition to the two orthogonal LP_{01} modes, at shorter wavelengths 'single-mode' fiber can propagate four LP_{11} modes.

the insertion of a short jumper cable or repair section, with a lateral offset, in a long single-mode fiber can excite the second-order LP_{11} mode [Ref. 44]. Moreover, such a repair section can also attenuate the fundamental LP_{01} mode if its operating wavelength is near the cutoff wavelength for this mode. Hence, to reduce modal noise, repair sections should use special fibers with a lower value of cutoff wavelength than that in the long single-mode fiber link; also offsets at joints should be minimized.

3.11 Overall fiber dispersion

3.11.1 Multimode fibers

The overall dispersion in multimode fibers comprises both chromatic and intermodal terms. The total rms pulse broadening σ_T is given (see Appendix D) by:

$$\sigma_T = (\sigma_c + \sigma_n)^{1/2} \tag{3.44}$$

where σ_c is the intramodal or chromatic broadening and σ_n is the intermodal broadening caused by delay differences between the modes (i.e. σ_s for multimode step index fiber and σ_g for multimode graded index fiber). The chromatic term σ_c consists of pulse broadening due to both material and waveguide dispersion. However, since waveguide dispersion is generally negligible compared with material dispersion in multimode fibers, then $\sigma_c \approx \sigma_m$.

Example 3.10

A multimode step index fiber has a numerical aperture of 0.3 and a core refractive index of 1.45. The material dispersion parameter for the fiber is 250 ps nm^{-1} km^{-1} which makes material dispersion the totally dominating chromatic dispersion mechanism. Estimate (a) the total rms pulse broadening per kilometer when the fiber is used with an LED source of rms spectral width 50 nm and (b) the corresponding bandwidth-length product for the fiber.

Solution: (a) The rms pulse broadening per kilometer due to material dispersion may be obtained from Eq. (3.18), where:

$$\sigma_m(1\text{ km}) \approx \frac{\sigma_\lambda L}{c}\left|\frac{d^2 n_1}{d\lambda^2}\right| = \sigma_\lambda LM = 50 \times 1 \times 250 \text{ ps km}^{-1}$$
$$= 12.5 \text{ ns km}^{-1}$$

The rms pulse broadening per kilometer due to intermodal dispersion for the step index fiber is given by Eq. (3.35) as:

$$\sigma_s\,(1\text{ km}) \quad \frac{L(NA)^2}{4\sqrt{3}n_1 c} = \frac{10^3 \times 0.09}{4\sqrt{3} \times 1.45 \times 2.998 \times 10^8} =$$

$$29.9\text{ ns km}^{-1}$$

The total rms pulse broadening per kilometer may be obtained using Eq. (3.43), where $\sigma_c \approx \sigma_m$ as the waveguide dispersion is negligible and $\sigma_n = \sigma_s$ for the multimode step index fiber. Hence:

$$\sigma_T = (\sigma_{2m} + \sigma_s)^{1/2} = (12.5^2 + 29.9^2)^{1/2}$$
$$= 32.4\text{ ns km}^{-1}$$

(b) The bandwidth-length product may be estimated from the relationship given in Eq. (3.11) where:

$$B_{opt} \times L = \frac{0.2}{\sigma_T} = \frac{0.2}{32.4 \times 10^{-9}}$$
$$= 6.2\text{ MHz km}$$

3.11.2 Single-mode fibers

The pulse broadening in single-mode fibers results almost entirely from chromatic or intramodal dispersion as only a single-mode is allowed to propagate.* Hence the bandwidth is limited by the finite spectral width of the source. Unlike the situation in multimode fibers, the mechanisms giving chromatic dispersion in single-mode fibers tend to be interrelated in a complex manner. The transit time or specific group delay τ_g for a light pulse propagating along a unit length of single-mode fiber may be given, following Eq. (2.107), as:

$$\tau_g = \frac{1}{c}\frac{d\beta}{dk} \tag{3.45}$$

where c is the velocity of light in a vacuum, β is the propagation constant for a mode within the fiber core of refractive index n_1 and k is the propagation constant for the mode in a vacuum.

The total first-order dispersion parameter or the chromatic dispersion of a single-mode fiber, D_T, is given by the derivative of the specific group delay with respect to the vacuum wavelength λ as:

$$D_T = \frac{d\tau_g}{d\lambda} \tag{3.46}$$

* Polarization mode dispersion can, however, occur in single-mode fibers (see Section 3.13.2).

In common with the material dispersion parameter it is usually expressed in units of ps nm^{-1} km^{-1}. When the variable λ is replaced by ω, then the total dispersion parameter becomes:

$$D_T = -\frac{\omega}{\lambda}\frac{d\tau_g}{d\omega} = -\frac{\omega}{\lambda}\frac{d^2\beta}{d\omega^2} \tag{3.47}$$

The fiber exhibits intramodal dispersion when β varies nonlinearly with wavelength. From Eq. (2.71) β may be expressed in terms of the relative refractive index difference Δ and the normalized propagation constant b as:

$$\beta = kn_1[1 - 2\Delta(1 - b)]^{1/2} \tag{3.48}$$

The rms pulse broadening caused by chromatic dispersion down a fiber of length L is given by the derivative of the group delay with respect to wavelength as [Ref. 45]:

$$\text{Total rms pulse broadening} = \sigma_\lambda L \frac{d\tau_g}{d\lambda} = \frac{\sigma_\lambda L}{c}\frac{2\pi}{\lambda^2}\frac{d^2\beta}{dk^2} \tag{3.49}$$

where σ_λ is the source rms spectral linewidth centered at a wavelength λ.

When Eq. (3.44) is substituted into Eq. (3.45), detailed calculation of the first and second derivatives with respect to k gives the dependence of the pulse broadening on the fiber material's properties and the normalized propagation constant b. This gives rise to three interrelated effects which involve complicated cross-product terms. However, the final expression may be separated into three composite dispersion components in such a way that one of the effects dominates each term [Ref. 46]. The dominating effects are as follows:

1. The material dispersion parameter D_M defined by $\lambda/c \mid d^2n/d\lambda^2 \mid$ where $n = n_1$ or n_2 for the core or cladding respectively.
2. The waveguide dispersion parameter D_W, which may be obtained from Eq. (3.47) by substitution from Eq. (2.114) for τ_g, is defined as:*

$$D_W = -\frac{A}{D}\frac{n_1 - n_2}{C\ \lambda c\ F} V\frac{d^2(Vb)}{dV^2} \tag{3.50}$$

where V is the normalized frequency for the fiber. Since the normalized propagation constant b for a specific fiber is only dependent on V, then the normalized

* Equation (3.50) does not provide the composite waveguide dispersion term (i.e. taking into account both the fiber core and the cladding) from which it differs by a factor near unity which contains $dn_2/d\lambda$ [Ref. 47].

waveguide dispersion coefficient $V\mathrm{d}^2(Vb)/\mathrm{d}V^2$ also depends on V. This latter function is another universal parameter which plays a central role in the theory of singlemode fibers.

3. A profile dispersion parameter D_P which is proportional to $\mathrm{d}\Delta/\mathrm{d}\lambda$.

This situation is different from multimode fibers where the majority of modes propagate far from cutoff and hence most of the power is transmitted in the fiber core. In the multimode case the composite dispersion components may be simplified and separated into two chromatic terms which depend on either material or waveguide dispersion, as was discussed in Section 3.9. Also, especially when considering step index multimode fibers, the effect of profile dispersion is negligible. Although material and waveguide dispersion tend to be dominant in single-mode fibers, the composite profile should not be ignored. However, the profile dispersion parameter D_P can be quite small (e.g. less than 0.5 ps nm^{-1} km^{-1}), especially at long wavelengths, and hence is often neglected in rough estimates of total dispersion within single-mode fibers.

Strictly speaking, in single-mode fiber with a power-law refractive index profile the composite dispersion terms should be employed [Ref. 47]. Nevertheless, it is useful to consider the total first-order dispersion D_T in a practical single-mode fiber as comprising:

$$D_T = D_M + D_W + D_P \qquad (\mathrm{ps\ nm^{-1}\ km^{-1}}) \tag{3.51}$$

which is simply the addition of the material dispersion D_M, the waveguide dispersion D_W and the profile dispersion D_P components. However, in standard single-mode fibers the total dispersion tends to be dominated by the material dispersion of fused silica. This parameter is shown plotted against wavelength in Figure 3.10. It may be observed that the characteristic goes through zero at a wavelength of 1.27 μm. This zero material dispersion (ZMD) point can be shifted anywhere in the wavelength range 1.2 to 1.4 μm by the addition of suitable dopants. For instance, the ZMD point shifts from 1.27 μm to approximately 1.37 μm as the GeO_2 dopant concentration is increased from 0 to 15%. However, the ZMD point alone does not represent a point of zero pulse broadening since the pulse dispersion is influenced by both waveguide and profile dispersion.

With ZMD the pulse spreading is dictated by the waveguide dispersion coefficient $V\mathrm{d}^2(Vb)/\mathrm{d}V^2$, which is illustrated in Figure 3.15 as a function of normalized frequency for the LP_{01} mode. It may be seen that in the single-mode region where the normalized frequency is less than 2.405 (see Section 2.5) the waveguide dispersion is always positive and has a maximum at $V = 1.15$. In this case the waveguide dispersion goes to zero outside the true single-mode region at $V = 3.0$. However, a change in the fiber parameters (such as core radius) or in the operating wavelength alters the normalized frequency and therefore the waveguide dispersion.

The total fiber dispersion, which depends on both the fiber material composition and dimensions, may be minimized by trading off material and waveguide dispersion while limiting the profile dispersion (i.e. restricting the variation in refractive index with wavelength). For wavelengths longer than the ZMD point, the material dispersion parameter is positive whereas the waveguide dispersion parameter is negative, as shown in Figure 3.16. However, the total dispersion D_T is approximately equal to the sum of the material dispersion D_M and the waveguide dispersion D_W following Eq. (3.50). Hence for a particular

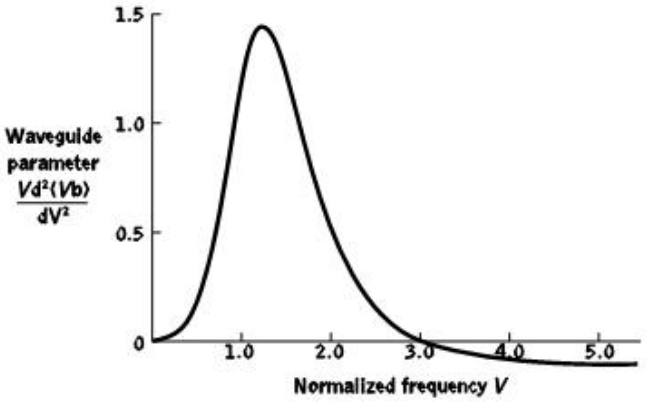

Figure 3.15 The waveguide parameter $V\,d^2(Vb)/dV^2$ as a function of the normalized frequency V for the LP_{01} mode. Reproduced with permission from W. A. Gambling. A. H. Hartog and C. M. Ragdale, *The Radio Electron. Eng.*, 51, p. 313, 1981

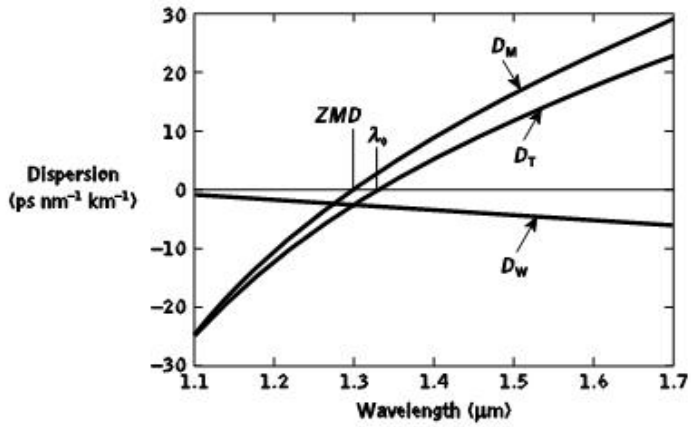

Figure 3.16 The material dispersion parameter (D_M), the waveguide dispersion parameter (D_W) and the total dispersion parameter (D_T) as functions of wavelength for a conventional single-mode fiber

wavelength, designated λ_0, which is slightly larger than the ZMD point wavelength, the waveguide dispersion compensates for the material dispersion and the total first-order dispersion parameter D_T becomes zero (see Figure 3.16). The wavelength at which the firstorder dispersion is zero, λ_0, may be selected in the range 1.3 to 2 μm by careful control of the fiber core diameter and profile [Ref. 46]. This point is illustrated in Figure 3.17 where the total first-order dispersion as a function of wavelength is shown for three single-mode fibers with core diameters of 4, 5 and 6 μm.

The effect of the interaction of material and waveguide dispersion on λ_0 is also demonstrated in the dispersion against wavelength characteristics for a single-mode silica core fiber shown in Figure 3.18. It may be noted that the ZMD point occurs at a wavelength of

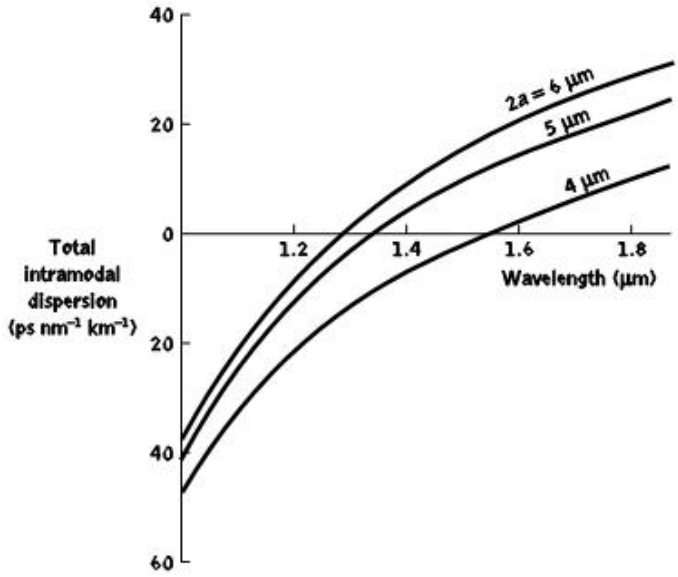

Figure 3.17 The total first order intramodal dispersion as a function of wavelength for single-mode fibers with core diameters of 4, 5, and 6 μm. Reproduced with permission from W. A. Gambling. A. H. Hartog, and C. M. Ragdale, *The Radio and Electron. Eng.*, 51, p. 313, 1981

1.276 μm for pure silica, but that the influence of waveguide dispersion shifts the total dispersion minimum towards the longer wavelength giving a λ_0 of 1.32 μm.

The wavelength at which the first-order dispersion is zero λ_0 may be extended to wavelengths of 1.55 μm and beyond by a combination of three techniques. These are:

(a) lowering the normalized frequency (V value) for the fiber;

(b) increasing the relative refractive index difference Δ for the fiber;

(c) suitable doping of the silica with germanium.

This allows bandwidth-length products for such single-mode fibers to be in excess of 100 GHz km^{-1} [Ref. 48] at the slight disadvantage of increased attenuation due to Rayleigh scattering within the doped silica.

For standard single-mode fibers optimized for operation at a wavelength of 1.31 μm, their performance characteristics are specified by the International Telecommunications Union ITU-T Recommendation G.652 [Ref. 49]. A typical example exhibits C-band (1.530 to 1.565 μm) total first-order chromatic dispersion D_T in the range 16 to 19 ps nm^{-1} km^{-1} with a zero-dispersion wavelength λ_0 between 1.302 and 1.322 μm. However, although the wavelength of zero first-order chromatic dispersion (i.e. $D_T = 0$) is often called the zero-dispersion wavelength, it is more correct to refer to it as the wavelength of minimum dispersion because of the significant second-order effects.

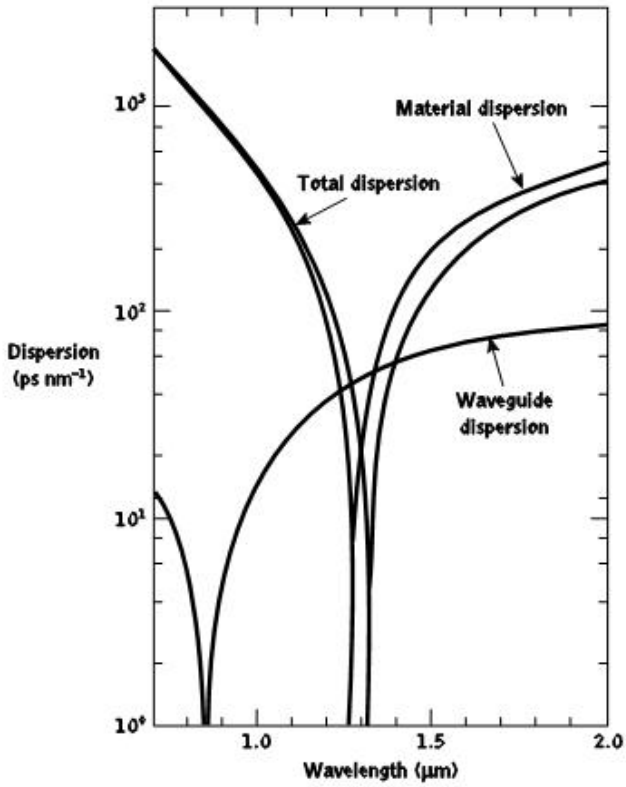

Figure 3.18 The pulse dispersion as a function of wavelength in 11 km single-mode fiber showing the major contributing dispersion mechanisms (dashed and dotted curves) and the overall dispersion (solid curve). Reprinted with permission from J. I. Yamada, M. Saruwatari, K. Asatani, H. Tsuchiya, A. Kawana, K. Sugiyama and T. Kumara, 'High speed optical pulse transmission at 1.29 μm wavelength using lowloss single-mode fibers', *IEEE J. Quantum Electron.*, QE-14, p. 791, 1978. Copyright © 1980, IEEE

The variation of the chromatic dispersion with wavelength is usually characterized by the second-order dispersion parameter or dispersion slope S which may be written as [Ref. 50]:

$$S = \frac{dD_T}{d\lambda} = \frac{d^2\tau_g}{d\lambda^2} \tag{3.52}$$

Whereas the first-order dispersion parameter D_T may be seen to be related only to the second derivative of the propagation constant β with respect to angular frequency in Eq. (3.47), the dispersion slope can be shown to be related to both the second and third derivatives [Ref. 47] following:

$$S = \frac{(2\pi c)^3}{\lambda^4}\frac{d^3\beta}{d\omega^3} + \frac{4\pi c}{\lambda^3}\frac{d^2\beta}{d\omega^2} \tag{3.53}$$

It should be noted that although there is zero first-order dispersion at λ_0, these higher order chromatic effects impose limitations on the possible bandwidths that may be achieved with single-mode fibers. For example, a fundamental lower limit to pulse spreading in silica-based fibers of around 2.50×10^{-2} ps nm^{-1} km^{-1} is suggested at a wavelength of 1.273 μm [Ref. 51]. These secondary effects, such as birefringence arising from ellipticity or mechanical stress in the fiber core, are considered further in Section 3.13. However, they may cause dispersion, especially in the case of mechanical stress of between 2 and 40 ps km^{-1}. If mechanical stress is avoided, pulse dispersion around the lower limit may be obtained in the longer wavelength region (i.e. 1.3 to 1.7 μm). By contrast the minimum pulse spread at a wavelength of 0.85 μm is around 100 ps nm^{-1} km^{-1} [Ref. 35].

An important value of the dispersion slope $S(\lambda)$ is obtained at the wavelength of minimum chromatic dispersion λ_0 such that:

$$S_0 = S(\lambda_0) \tag{3.54}$$

where S_0 is called the zero-dispersion slope which, from Eqs (3.46) and (3.52), is determined only by the third derivative of β. Typical values for the dispersion slope for standard single-mode fiber at λ_0 are in the region 0.085 to 0.095 ps nm^{-1} km^{-1}. The total chromatic dispersion at an arbitrary wavelength can be estimated when the two parameters λ_0 and S_0 are specified according to [Ref. 52]:

$$D_T(\lambda) = \frac{\lambda S_0}{4}\left[1 - \left(\frac{\lambda_0}{\lambda}\right)^4\right] \tag{3.55}$$

Example 3.11

A typical single-mode fiber has a zero-dispersion wavelength of 1.31 μm with a dispersion slope of 0.09 ps nm^{-2} km^{-1}. Compare the total first-order dispersion for the fiber at the wavelengths of 1.28 μm and 1.55 μm. When the material dispersion and profile dispersion at the latter wavelength are 13.5 ps nm^{-1} km^{-1} and 0.4 ps nm^{-1} km^{-1}, respectively, determine the waveguide dispersion at this wavelength.

Solution: The total first-order dispersion for the fiber at the two wavelengths may be obtained from Eq. (3.55). Hence:

$$D_T(1280\text{ nm}) = \frac{\lambda S_0}{4}\left[1 - \left(\frac{\lambda_0}{\lambda}\right)^4\right]$$

$$= \frac{1280 \times 0.09 \times 10^{-12}}{4}\left[1 - \left(\frac{1310}{1280}\right)^4\right]$$

$$= -2.8 \text{ ps nm}^{-1} \text{ km}^{-1}$$

and:

$$D_T(1550\text{ nm}) = \frac{1550 \times 0.09 \times 10^{-12}}{4}\left[1 - \left(\frac{1310}{1550}\right)^4\right]$$

$$= 17.1\text{ ps nm}^{-1}\text{ km}^{-1}$$

The total dispersion at the 1.28 μm wavelength exhibits a negative sign due to the influence of the waveguide dispersion. Furthermore, as anticipated the total dispersion at the longer wavelength (1.55 μm) is considerably greater than that obtained near the zero-dispersion wavelength.

The waveguide dispersion for the fiber at a wavelength of 1.55 μm is given by Eq. (3.51) where:

$$D_W = D_T - (D_M + D_P)$$
$$= 17.1 - (13.5 + 0.4)$$
$$= 3.2\text{ ps nm}^{-1}\text{ km}^{-1}$$

3.12 Dispersion-modified single-mode fibers

It was suggested in Section 3.11.2 that it is possible to modify the dispersion characteristics of single-mode fibers by the tailoring of specific fiber parameters. However, the major trade-off which occurs in this process between material dispersion (Eq. 3.19) and waveguide dispersion (Eq. 3.50) may be expressed as:

$$D_T = D_M + D_W = \underbrace{\frac{\lambda}{c}\frac{d^2 n_1}{d\lambda^2}}_{\text{material dispersion}} - \underbrace{\left[\frac{n_1 - n_2}{\lambda c}\right]\frac{d^2(Vb)}{dV^2}}_{\text{waveguide dispersion}} \tag{3.56}$$

At wavelengths longer than the ZMD point in most common fiber designs, the D_M and D_W components are of opposite sign and can therefore be made to cancel at some longer wavelength. Hence the wavelength of zero first-order chromatic dispersion can be shifted to the lowest loss wavelength for silicate glass fibers at 1.55 μm to provide both lowdispersion and low-loss fiber. This may be achieved by such mechanisms as a reduction in the fiber core diameter with an accompanying increase in the relative or fractional index difference to create so-called dispersion-shifted single-mode fibers (DSFs). However, the design flexibility required to obtain particular dispersion, attenuation, mode-field diameter and bend loss characteristics has resulted in specific, different refractive index profiles for these dispersion-modified fibers [Ref. 53].

An alternative modification of the dispersion characteristics of single-mode fibers involves the achievement of a low-dispersion window over the low-loss wavelength region between 1.3 and 1.6 μm. Such fibers, which relax the spectral requirements for

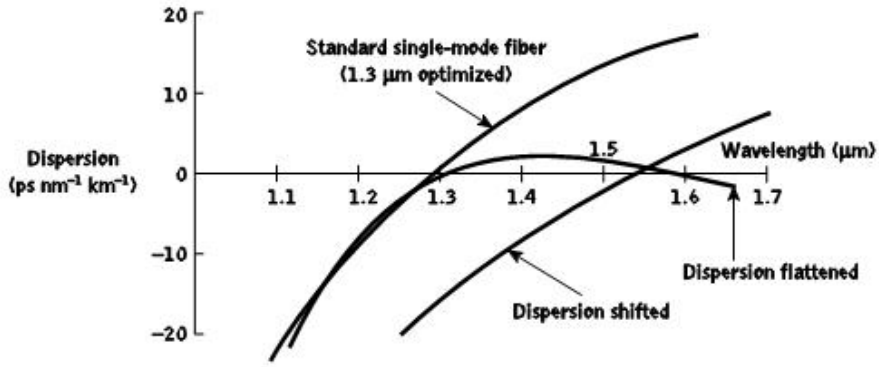

Figure 3.19 Total dispersion characteristics for the various types of single-mode fiber

optical sources and allow flexible wavelength division multiplexing (see Section 12.9.4) are known as dispersion-flattened single-mode fibers (DFFs). In order to obtain DFFs multilayer index profiles are fabricated with increased waveguide dispersion which is tailored to provide overall dispersion (e.g. less than 2 ps nm^{-1} km^{-1}) over the entire wavelength range 1.3 to 1.6 μm [Ref. 54]. In effect these fibers exhibit two wavelengths of zero total chromatic dispersion. This factor may be observed in Figure 3.19 which shows the overall dispersion characteristics as a function of optical wavelength for standard single-mode fiber (SSMF) optimized for operation at 1.3 μm in comparison with both DSF and DFF [Ref. 55]. Furthermore, the low-water-peak fiber discussed in Section 3.3.2 currently exhibits overall dispersion characteristics that are the same as those for the SSMF shown in Figure 3.19. It should also be noted that although DFF is characterized by low dispersion over a large wavelength range, it has been superseded by nonzero dispersion-shifted fiber (see Section 3.12.3) and therefore it does not currently find use in practical applications.

3.12.1 Dispersion-shifted fibers

A wide variety of single-mode fiber refractive index profiles are capable of modification in order to tune the zero-dispersion wavelength point λ_0 to a specific wavelength within a region adjacent to the ZMD point. In the simplest case, the step index profile illustrated in Figure 3.20 gives a shift to longer wavelength by reducing the core diameter and increasing the fractional index difference. Typical values for the two parameters are 4.4 μm and 0.012 respectively [Ref. 56]. For comparison, the standard nonshifted design is shown dashed in Figure 3.20.

It was indicated in Section 3.11.2 that λ_0 could be shifted to longer wavelength by altering the material composition of the single-mode fiber. For suitable power confinement of the fundamental mode, the normalized frequency V should be maintained in the range 1.5 to 2.4 μm and the fractional index difference must be increased as a square function while the core diameter is linearly reduced to keep V constant. This is normally achieved by substantially increasing the level of germanium doping in the fiber core. Figure 3.21 [Ref. 56] displays typical material and waveguide dispersion characteristics for single-mode step

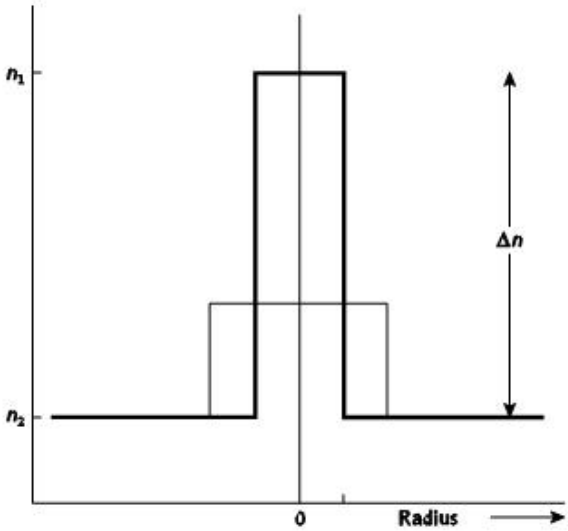

Figure 3.20 Refractive index profile of a step index dispersion-shifted fiber (solid) with a conventional nonshifted profile design (dashed)

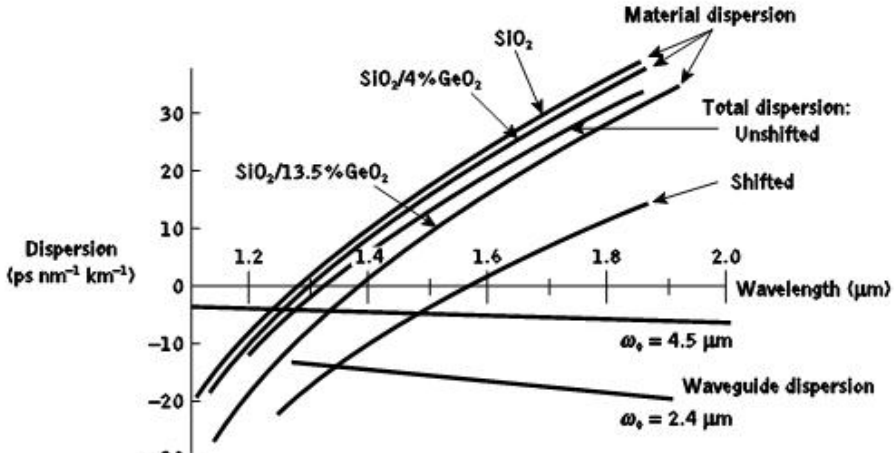

Figure 3.21 Material, waveguide and total dispersion characteristics for conventional and dispersion-shifted step index single-mode fibers showing variation with
composition and spot size (ω_0)

index fibers with various compositions and core radii. It may be observed that higher concentrations of the dopant cause a shift to longer wavelength which, when coupled with a reduction in the mode-field diameter (MFD), giving a larger value (negative of waveguide dispersion), leads to the shifted fiber characteristic shown in Figure 3.21.

A problem that arises with the simple step index approach to dispersion shifting displayed in Figure 3.20 is that the fibers produced exhibit relatively high dopant-dependent

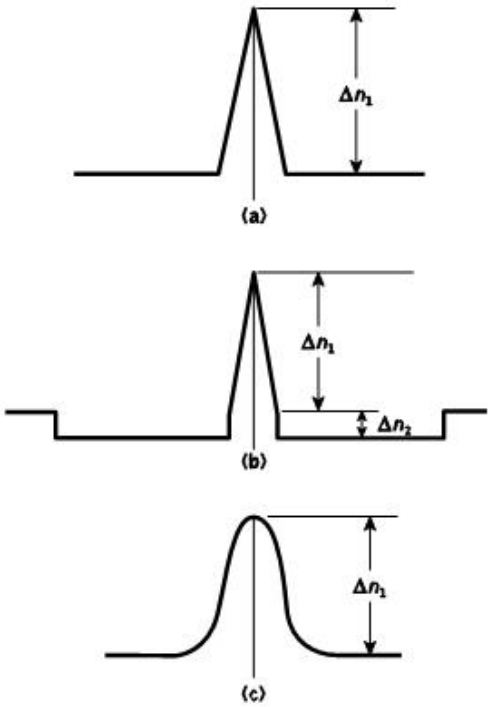

Figure 3.22 Refractive index profiles for graded index dispersion-shifted fibers: (a) triangular profile; (b) depressed-cladding triangular profile; (c) Gaussian profile

losses at operation wavelengths around 1.55 μm. This excess optical loss, which may be of the order of 2 dB km^{-1} [Ref. 56], could be caused by stress-induced defects which occur in the region of the core-cladding interface [Ref. 57]. Alternatively, it may result from refractive index inhomogeneities associated with waveguide variations at the core-cladding interface [Ref. 58]. A logical assumption is that any stress occurring across the core-cladding interface might be reduced by grading the material composition and therefore an investigation of graded index single-mode fiber designs was undertaken.

Several of the graded refractive index profile DSF types are illustrated in Figure 3.22. The triangular profile shown in Figure 3.22(a) is the simplest and was the first to exhibit the same low loss (i.e. 0.24 dB km^{-1}) at a wavelength of 1.56 μm (i.e. λ_0) as conventional nonshifted single-mode fiber [Ref. 59]. Furthermore, such fiber designs also provide an increased MFD over equivalent step index structures which assists with fiber splicing [Ref. 56]. However, in the basic triangular profile design the optimum parameters giving low loss together with zero dispersion at a wavelength of 1.55 μm cause the LP_{11} mode to cut off in the wavelength region 0.85 to 0.9 μm. Thus the fiber must be operated far from cutoff, which produces sensitivity to bend-induced losses (in particular microbending) at the 1.55 μm wavelength [Ref. 60]. One method to overcome this drawback is to employ a triangular index profile combined with a depressed cladding index, as shown in Figure 3.22(b) [Ref. 61]. In this case the susceptibility to microbending losses is reduced through a shift of the LP_{11} cutoff wavelength to around 1.1 μm with an MFD of 7 μm at 1.55 μm.

Low losses and zero dispersion at a wavelength of 1.55 μm have also been obtained with a Gaussian refractive index profile, as illustrated in Figure 3.22(c). This profile, which was achieved using the vapor axial deposition fabrication process (see Section 4.4.2), produced losses of 0.21 dB km^{-1} at the λ_0 wavelength of 1.55 μm [Ref. 62].

The alternative approach for the production of DSF has involved the use of multiple index designs. One such fiber type which has been used to demonstrate dispersion shifting but which has been more widely employed for DFFs (see Section 3.12.2) is the doubly clad or W fiber (see Section 2.5). However, the multiple index triangular profile fibers [Ref. 63] and the segmented-core triangular profile designs [Ref. 64], which are shown in Figure 3.23(a) and (b), respectively, have reduced the sensitivity to microbending by shifting the LP_{11} mode cutoff to longer wavelength while maintaining an MFD of around 9 μm at a wavelength of 1.55 μm. The latter technique of introducing a ring of elevated index around the triangular core enhances the guidance of the LP_{11} mode towards longer wavelength. Such fibers may be obtained as commercial products and have been utilized within the telecommunication network [Ref. 65], exhibiting losses as low as 0.17 dB at 1.55 μm [Ref. 66].

Dual-shaped core DSFs have also come under investigation in order to provide an improvement in bend loss performance over the 1.55 μm wavelength region [Refs 67, 68]. A dual-shaped core refractive index profile is shown in Figure 3.23(c), which illustrates a step index fiber design.

DSF has more recently been subject to the standardization recommendation ITU-T G.653 [Ref. 69]. Typical values for its attenuation are in the range 0.22 to 0.24 dB km^{-1} while it exhibits dispersion between 0 and 2.7 ps nm^{-1} km^{-1}, both at a wavelength of 1.55 μm. Although DSF has been installed to provide for high-speed transmission of a single 1.55 μm wavelength channel, it presents dispersion problems for wavelength division multiplexed operation when many wavelength channels are packed into one or more of the ITU spectral bands (see Section 3.3.2). In particular, as all the transmitted channels need to be grouped around the 1.55 μm wavelength to reduce dispersion, they then travel at the same speed creating four-wave mixing interaction and the associated high crosstalk levels (see Section 3.14.2). Hence DSF is no longer recommended for deployment.

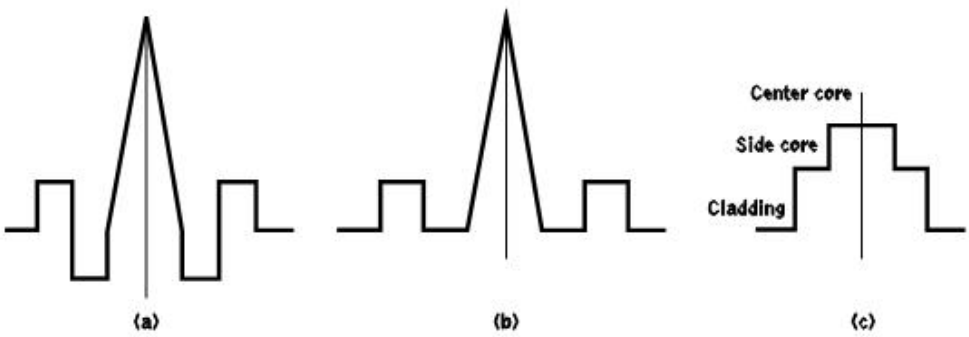

Figure 3.23 Advanced refractive index profiles for dispersion-shifted fibers: (a) triangular profile multiple index design; (b) segmented-core triangular profile design; (c) dual-shaped core design

3.12.2 Dispersion-flattened fibers

The original W fiber structure mentioned in Section 3.12.1 was initially employed to modify the dispersion characteristics of single-mode fibers in order to give two wavelengths of zero dispersion, as illustrated in Figure 3.19. A typical W fiber index profile (double clad) is shown in Figure 3.24(a). The first practical demonstration of dispersion flattening using the W structure was reported in 1981 [Ref. 70]. However, drawbacks with the W structural design included the requirement for a high degree of dimensional control so as to make reproducible DFF [Ref. 71], comparatively high overall fiber losses (around 0.3 dB km^{-1}), as well as a very high sensitivity to fiber bend losses. The last factor results from operation very close to the cutoff (or leakage) of the fundamental mode in the long-wavelength window in order to obtain a flat dispersion characteristic.

To reduce the sensitivity to bend losses associated with the W fiber structure, the light which penetrates into the outer cladding area can be retrapped by introducing a further region of raised index into the structure. This approach has resulted in the triple clad (TC) and quadruple clad (QC) structures shown in Figure 3.24(b) and (c) [Refs 72, 73]. An independent but similar program produced segmented-core DFF designs [Ref. 66].
Although reports of low attenuation of 0.19 dB km^{-1} for DFF at a wavelength of 1.55 μm [Ref. 74] with significantly reduced bending losses [Ref. 75] have been made, it has proved difficult to balance the performance attributes of this fiber type.

More recent efforts have focused on DFFs that exhibit low-dispersion slopes in the C-band while also providing acceptably large effective core areas in order to reduce fiber nonlinear effects [Ref. 76]. It is particularly difficult, however, to realize both near-zero-dispersion slopes and large effective core areas while, in addition, reducing their current bend loss sensitivity. Furthermore, there remain some fundamental problems associated with DFF fabrication as the chromatic dispersion characteristics are highly dependent on changes in the fiber structural parameters including the core diameter and refractive index difference. It is therefore still a concern that commercial production of DFFs will require both substantial stability and controllability of the fabrication process [Ref. 77]. Hence such fibers have yet to find widespread deployment in telecommunication networks.

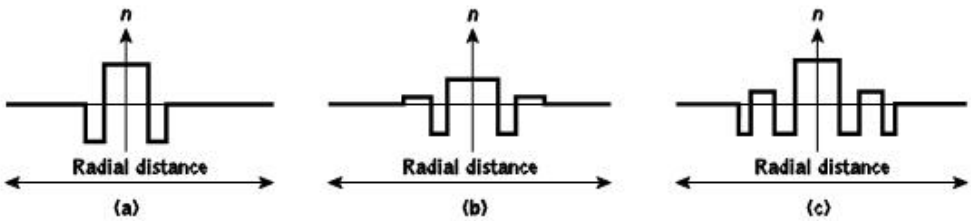

Figure 3.24 Dispersion-flattened fiber refractive index profiles: (a) double clad fiber (W fiber); (b) triple clad fiber; (c) quadruple clad fiber

3.12.3 Nonzero-dispersion-shifted fibers

Nonzero-dispersion-shifted fiber (NZ-DSF) is sometimes simply called nonzero-dispersion fiber (NZDF) and a variant of this fiber type is negative-dispersion fiber (NDF)

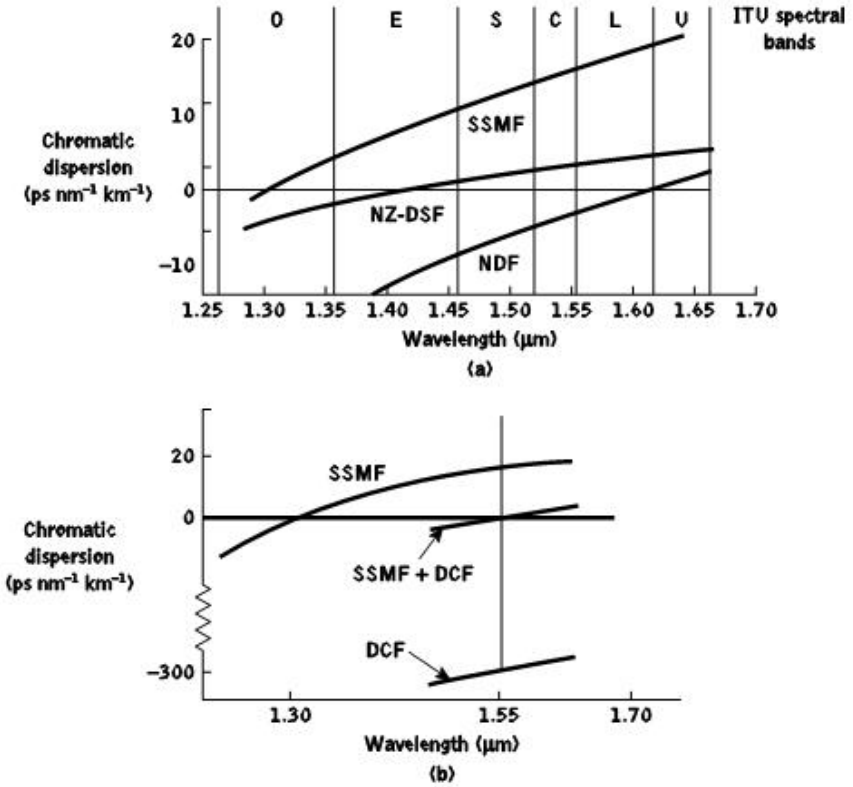

Figure 3.25 Single-mode fiber dispersion characteristics: (a) comparing the profiles for nonzero-dispersion-shifted fiber (NZ-DSF) and negative-dispersion fiber (NDF) with standard single-mode fiber (SSMF); (b) dispersion compensation by using negative-dispersion, dispersion-compensating fiber (DCF)

which can also be referred to as dispersion compensating fiber (DCF). NZ-DSF was introduced in the mid-1990s to better provide for wavelength division multiplexing applications (see Section 12.9.4). It is specified in the ITU-T Recommendation G.655 [Ref. 78] in which, unlike DSF, its principal attribute is that it has a nonzero-dispersion value over the entire C-band as may be observed from the dispersion characteristic profile displayed in Figure 3.25(a). In comparison, however, with the SSMF profile also shown in Figure 3.25(a), the chromatic dispersion exhibited by NZ-DSF at a wavelength of 1.55 μm is much lower, being in the range 2 to 4 ps nm^{-1} km^{-1} rather than the typical 17 ps nm^{-1} km^{-1} for SSMF.

It should also be noted that the dispersion profile for NZ-DSF shown in Figure 3.25(a) is also referred to as extended band or bandwidth nonzero-dispersion-shifted fiber which was introduced in 2000 to enable wavelength division multiplexed applications to be extended into the S-band. Hence it can be seen that it exhibits nonzero dispersion over the full C- and S-bands, whereas with the original NZ-DSF the dispersion varies from negative values through zero to positive values in the S-band. In addition, Figure 3.25(a) also

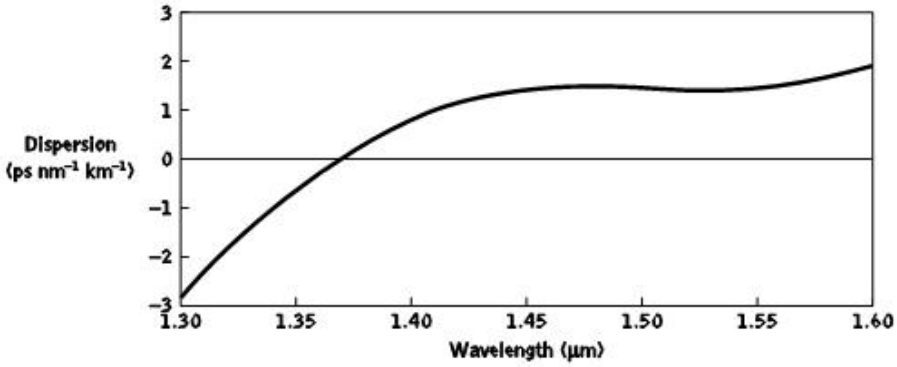

Figure 3.26 Flattened dispersion spectrum for an extended band NZ-DSF

displays the dispersion profile for NDF,* which exhibits negative dispersion over the entire 1.30 to 1.60 μm wavelength range (E-, S- and C-bands) as its dispersion zero is shifted to around 1.62 μm. Such fiber facilitates dispersion compensation when used together with either SSMF or NZ-DSF, both of which have positive dispersion over the majority of the aforementioned spectral range. The dispersion compensation attribute of negative-dispersion fiber identified as dispersion compensating fiber (DCF) is illustrated in the dispersion characteristic shown in Figure 32.5(b) where the total chromatic dispersion accumulated in the SSMF is cancelled by inserting an appropriate length of DCF (often exhibiting large absolute dispersion around -300 ps nm^{-1} km^{-1}) which provides the equivalent total negative dispersion, thus giving zero overall dispersion at the 1.55 μm wavelength on the transmission link.

The dispersion characteristic for an extended band NZ-DSF can also be flattened, as indicated in Figure 3.26, which then provides low, but noticeable, dispersion in S- and C-bands, further reducing the nonlinear crosstalk problem associated with four-wave mixing. This reduction in the dispersion slope or flattening is an important issue in the design of extended band NZ-DSFs together with the enlargement of the effective core area. The former adjusts the chromatic dispersion to appropriate levels across a wide wavelength range while the latter is intended to suppress the nonlinear effects in the fiber (see Section 3.14). Pursuing both these objectives produces a trade-off in the fiber design process which has resulted in a number of refractive index profiles being explored to improve the performance of NZ-DSF.

The refractive index profiles shown in Figure 3.23(b) and (c) for DSF have also been utilized to provide NZ-DSF. Indeed, the segmented core triangular profile displayed in Figure 3.23(b) is employed by the commercially produced Corning LEAF fiber which exhibits a large effective core area at the expense of a high-dispersion slope. A more typical NZ-DSF multiple index profile is shown in Figure 3.27(a) whereas a NDF refractive index profile is illustrated in Figure 3.27(b).

Although NZ-DSF has now effectively replaced both DSF and DFF for use in long-haul optical fiber communications in order to remove four-wave mixing crosstalk with multichannel operation, it is still subject to greater problems with nonlinearities in

* An example is the Corning MetroCor fiber.

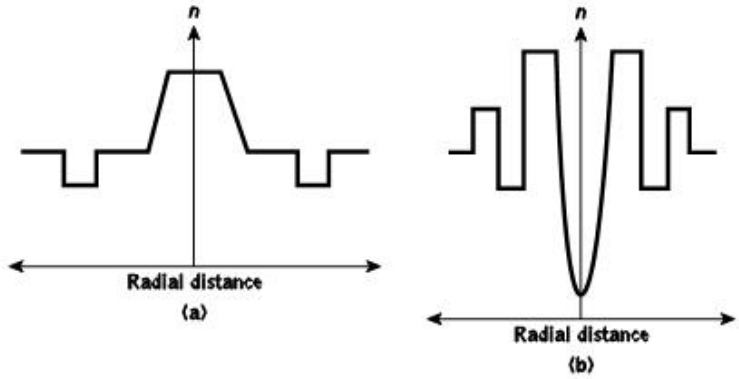

Figure 3.27 Typical refractive index profiles: (a) nonzero-dispersion-shifted fiber (NZDSF); (b) negative-dispersion fiber (NDF)

Table 3.3 Typical performance parameters for common nonzero-dispersion-shifted fibers (NZ-DSFs) all at 1.55 μm, excepting the zero-dispersion wavelength [Ref. 77]

Parameter	*Reduced slope NZ-DSF*	*Large effective core NZ-DSF*	*Extended band NZ-DSF*
Zero-dispersion wavelength (μm)	1.46	1.50	1.42
Dispersion (ps nm^{-1} km^{-1})	4	4	8
Dispersion slope (ps nm^{-2} km^{-1})	0.045	0.085	0.058
Effective core area (μm^2)	50	70	63

comparison with SSMF. This situation occurs because in general NZ-DSF has a smaller cross-sectional area and therefore the nonlinear threshold power levels can be reached at lower values of transmitted power. To keep the ratio of power to effective area low, however, a so-called large effective area NZ-DSF can be used to lower the power density below that of a conventional NZ-DSF [Ref. 79]. A further advantage of the large effective area approach is that it provides improved splicing capability to SSMF.

Typical parameters for some common NZ-DSFs are summarized in Table 3.3 [Ref. 77]. It may be observed that NZ-DSF with a reduced dispersion slope exhibits a significantly smaller effective core area in comparison with the large effective core NZ-DSF and also the extended band NZ-DSF. Examples of a reduced dispersion slope and an extended band NZ-DSFs are the Lucent TrueWave-RS and the Alcatel TeraLight fibers respectively.